



Spatial-temporal variations of surface urban heat island: An application of local climate zone into large Chinese cities

Ran Wang^{a,*}, James Voogt^b, Chao Ren^c, Edward Ng^d

^a College of Economic and Social Development, Nankai University, Tianjin, China

^b Department of Geography and Environment, Western University, London, ON, Canada

^c Faculty of Architecture, The University of Hong Kong, Hong Kong, China

^d School of Architecture, The Chinese University of Hong Kong, Hong Kong, China

ARTICLE INFO

Keywords:

Surface urban heat island (SUHI)

Local climate zone (LCZ)

Spatial-temporal variation

Intra-urban variation

Urban heat mitigation

ABSTRACT

The land surface temperature (LST)—based surface urban heat island (SUHI) is suitable for exploring thermal environments at large scales. Despite a few studies focused on the intra-urban SUHI intensity (SUHII) of a single city or cities with similar climates by adopting the local climate zone (LCZ) scheme, exploration of the spatial-temporal characteristics of the intra-urban SUHII and SUHI extent (SUHIE) is still limited across diverse climate zones. This study aims to (1) propose an improved LCZ mapping method to refine historical LCZ data for highly urbanized Chinese cities; (2) put forward a buffer-based approach to quantify the actual area affected by the SUHI; (3) investigate the spatial-temporal pattern of SUHI in large Chinese cities. The results show that the intra-urban SUHII varies across seasons, times and background climate—highest during summer days and lowest during winter days, decreasing with background climate becoming warm and wet. SUHIE displays an apparent temporal pattern similar to SUHII and has an increasing trend, but it relates more to urban areas (particularly the area of LCZ 1) than background climate. Due to the positive impact of LCZ 1 on both SUHII and SUHIE, its area should be strictly restricted in design practice. Although LCZ 4 has the advantage over LCZ 1 in mitigating SUHII, it correlates positively to SUHI expansion. From a planning perspective, a balance between the reduction of SUHII and SUHIE should be considered. This study provides evidence-based planning recommendations to mitigate urban heat and create a comfortable built environment.

1. Introduction

The surface urban heat island (SUHI) effect, which refers to the surface temperature difference between urban and rural sites, is one of the environmental impacts of urbanization [1]. Compared to the air UHI effect, the land surface temperature (LST)-based SUHI effect is particularly suitable for monitoring thermal environments at a broad scale, like city/regional/continental/global scale [2]. China has a broad territory with diverse terrain and climates, rapid expansion of urban areas and variable socioeconomic levels across cities. Hence, the SUHI effect calculated by using satellite images provides a consistent approach to exploring the thermal environment of different Chinese cities. The SUHI affects energy consumption [3] and human health [4]. Comparing the urban to rural population ratio of China (60.6% in 2019) [5] with that of developed countries (80%) [6], there is still room for China to increase its urbanization level. Correspondingly, more populations will be

enveloped by the SUHI with ongoing urbanization. Therefore, it is necessary to explore the spatial-temporal variations of SUHIs in Chinese cities to create a comfortable living environment.

Previous SUHI-related studies usually calculated SUHI intensity (SUHII) as urban-rural LST difference, while definitions of “urban” and “rural” sites vary across different study areas and the simple one urban category homogenizes intra-urban difference of heat island [7]. To offer a standard site selection framework for UHI studies and link urban morphology with thermal properties, Stewart and Oke [7] proposed the Local Climate Zone (LCZ) classification system which includes ten built types and seven land cover types. Since the putting forward of the LCZ scheme, scholars have made efforts to map LCZs by using freely available remote sensing data and various classification algorithms [1,8–10]. World Urban Database and Access Portal Tool (WUDAPT) provides a city-scale LCZ mapping approach by using Landsat imagery and a random forest classifier [8], which has been applied to many cities

* Corresponding author., College of Economic and Social Development, Nankai University, No.94 Weijin Road, Nankai District, Tianjin, 300071, China.

E-mail address: wangran@nankai.edu.cn (R. Wang).

across the globe [11–13]. However, due to the considerable burdens of data storage and offline computation, such a city-by-city LCZ mapping approach may not be suitable for large-scale environmental studies (e.g., regional, national, and continental). To fill this gap, recent studies have employed Google Earth Engine (GEE) in LCZ mapping due to its parallel computational power, various geospatial datasets and predefined algorithms. GEE-based LCZ classification method has been employed to map LCZs in Guangdong-Hong Kong-Macau Great Bay Area of China [14], United States [15] and Europe [16]. These recent GEE-based LCZ classification methods use input data from one particular year [14] or two to three years [15,16] to produce one specific LCZ map. However, time-series LCZs are essential for the temporal analysis of UHIs and other urban climate studies, particularly in developing countries with rapid urbanization. Temporal consistency is a critical issue in time-series LCZ mapping, which means transformation from built type to natural landscape or from high-rise buildings to low-rise buildings seldomly occur [17]. Few LCZ mapping methods in previous studies took account of the temporal consistency of LCZs between different years. Considering the rapid urbanization process in China, it is necessary to ensure the temporal consistency of LCZs to provide a correct urban database for the subsequent formulation of planning strategies.

The fine-scale classification of urban categories in the LCZ scheme makes it possible to investigate the intra-urban thermal behavior. Studies have already adopted the LCZ scheme with LST to explore the intra-urban LST/SUHII variation in different cities or metropolitan areas, like Budapest in Hungary [11], Prague and Brno in the Czech Republic and Novi Sad in Serbia [1], Phoenix and Las Vegas in the USA [13], the Pearl River Delta (PRD) region of China [17], and the Yangtze River Delta (YRD) region in China [9]. Studies to date suggest that the use of LST has shown a reasonable ability to discriminate between LCZ classes, but the LCZ-LST/SUHII was mainly examined at the city or urban agglomeration scale, where the background climate has no significant difference. For instance, Dian et al. [11] used MODIS LST data to assess the summer and winter intra-urban SUHII of Budapest with a mid-latitude continental climate. They found that LCZ 2 performed the highest SUHII. Based on the single-year data, Cai et al. [9] explored the summertime LCZ-LST relationship in the YRD region with a subtropical monsoon climate; LCZ 1 was observed as the warmest LCZ type. The LCZ-SUHII relationship is supposed to vary with diverse background climates that primarily affect the rural surface. However, an exploration of how the intra-urban SUHII behaves across various climate zones is still limited.

The SUHI intensity has attracted much attention in analyzing spatial-temporal variations of the SUHI effect in China [18]. However, the SUHI intensity does not represent the spatial range of the actual heat variability in cities. Several domestic studies attempt to quantify the area affected by the SUHI by using the two-dimensional Gaussian surface model [2,19,20]. The basic idea of this method is that the spatial distribution of the SUHI can be fitted by a two-dimensional Gaussian surface. Streutker [21] first implemented the Gaussian surface model to analyze the temporal variations of SUHI footprints (spatial extent of the SUHI) in Houston, Texas, based on remote sensing images. However, the obtained spatial extent generated by the Gaussian surface model was a closed ellipse [2], which is often not a good match to the actual urban development pattern for a specific city. Besides, limited by its mathematical origin, the Gaussian surface model is only applicable to single-center urban expansion scenarios, while multi-center urban development has been emerging as a common expansion mode in Chinese cities. Hence, there is a knowledge gap in quantifying the SUHI extent (SUHIE) which fits urban development patterns.

The novelty of this research is that an improved LCZ mapping method and a new SUHIE quantifying approach are put forward, and spatial-temporal patterns of intra-urban SUHII and SUHIE and their relations to background climate are revealed. Research objectives of this paper include: (1) putting forward a GEE-based LCZ classification method that is suitable for time-series LCZ mapping, (2) proposing a

SUHIE quantifying approach that suits multicentric urban development, (3) analyzing spatial-temporal patterns of intra-urban SUHII and SUHIE, as well as quantifying their relationships to background climate, and (4) providing planning recommendations for creating cool communities. This study will fill the gaps of time-series LCZ mapping with temporal consistency, depicting SUHIE in agreement with actual urban development and quantifying the impact of background climate on intra-urban SUHII and SUHIE (i.e., spatial variability). Our findings will advance the understanding of SUHII and SUHIE from temporal and spatial perspectives and provide insights into urban heat mitigation from a detailed land use and land cover and urban morphological perspective.

2. Materials and methods

2.1. Study area

This study selects eight cities with a population of over five million as study targets. For the convenience of discussion, such cities are defined as large cities in this paper. The eight cities are all central cities for their urban agglomerations, serving as important economic, cultural, innovative and transportation centers. They all had experienced significant urbanization during the past few decades in urban populations and built-up areas (Table A1). Urbanization is projected to continue not only in China but also in the world [6]. Exploring heat islands in these highly urbanized cities can provide other cities undergoing urbanization with lessons and experiences in terms of LCZ-based heat island analysis and corresponding heat mitigation strategies. Besides, the eight large cities are located in seven geographical regions and four architectural climate zones [22] (Fig. 1, Table A1, Table A2). Cities in severe cold and cold regions are equipped with heating systems while those in relatively warm regions do not. Diverse geographical locations and climate zones make it possible to relate the intensity and extent of SUHI to climates in this study. The heat island effects of these cities are expected to have similarities and differences amongst one another.

The study period covers a part of the post-reform urbanization periods, starting from 2000 and ending in 2015, during which Chinese cities experienced rapid urbanization and socioeconomic development. LCZ maps and LST maps were generated in 2000, 2005, 2010 and 2015. The subsequent SUHI analysis was also conducted during three periods (2000–2005, 2005–2010, 2010–2015).

2.2. LCZ mapping

Based on GEE, this study developed an improved LCZ mapping method with a temporal consistency check. Multi-temporal LCZ maps

Table 1
Summary of input earth observation data for historical LCZ mapping.

Input features	Spatial resolution	Source with the acquisition time
Yearly and seasonal composite of spectral bands (B2-7, B10, B11 for Landsat 8, B1-7 for Landsat 5)	30 m	Landsat 5 (2000, 2005, 2010), Landsat 8 (2015)
Mean NDBaI, NDWI, NDBI	30 m	Landsat 5 (2000, 2005, 2010), Landsat 8 (2015)
Maximum, minimum, and mean NDVI	30 m	Landsat 5 (2000, 2005, 2010), Landsat 8 (2015)
DSM	1 arc (approximately 30 m)	AW3D30 (2006–2011), SRTM (2000)
DTM	7.5 arc (approximately 225 m)	GMTED (Fusion of different DEM data sources)
Canopy height (DSM-DTM)	30 m (resample DTM to 30 m)	AW3D30, GMTED

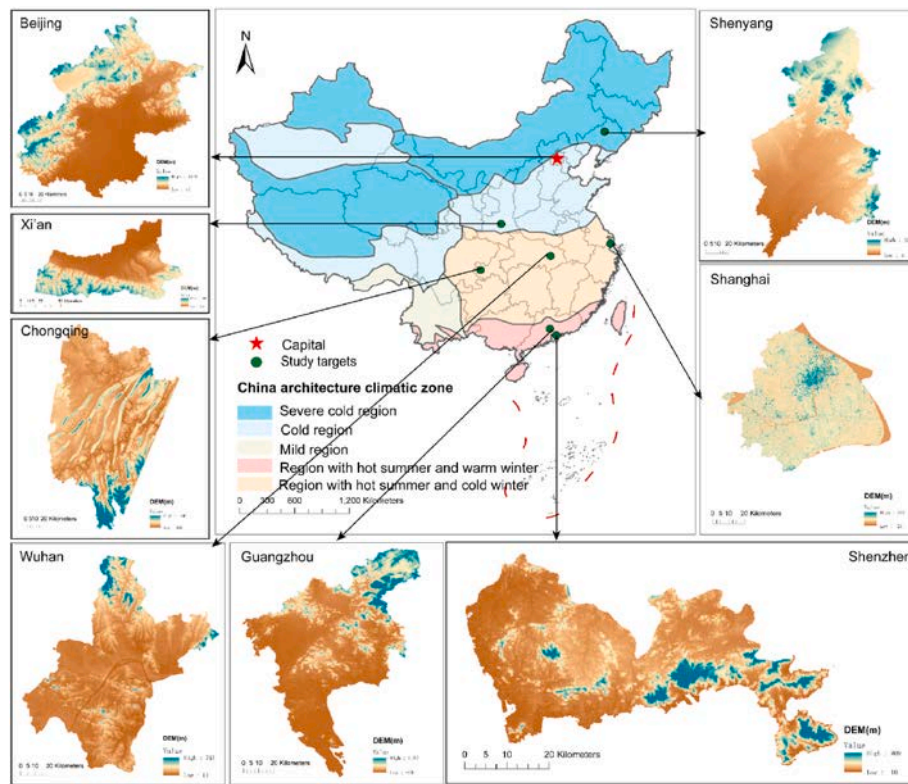


Fig. 1. Geographical location, terrain and China architectural climate zone* of eight large cities.

* Architectural climate zones are based on a classification system issued by the Government of China to help make buildings adaptive to local climates [23].

Table 2

Correlation coefficients between air temperature, precipitation, relative humidity, urban area and the SUHI extent during daytime and nighttime of summer and winter.

	AirT	P	RH	UA
Summer-daytime SUHIE	-0.166	-0.091	-0.390*	0.900*
Summer-nighttime SUHIE	-0.093	-0.008	-0.311	0.787*
Winter-daytime SUHIE	-0.060	0.138	-0.378*	0.866*
Winter-nighttime SUHIE	-0.024	0.206	-0.308	0.812*

Note: AirT—air temperature, P—precipitation, RH—relative humidity, UA—urban area.

* indicate two variables are significantly correlated at a significance level of 0.05.

with a 100-m resolution were produced at a city scale for eight large cities.

2.2.1. Input features

2.2.1.1. Earth observation datasets. Table 1 summarizes all input earth observation datasets used in multi-temporal LCZ mapping for this study. The input datasets can be classified into three categories—spectral bands, spectral indices and height information. First, the yearly and seasonal composites of Landsat spectral bands were employed to minimize the influence of a single Landsat image and seasonal changes in vegetation on the final classification result. Second, spectral indices were used to differentiate various land cover types, like vegetated surface, bare soil, impervious surface and water bodies, since the spectral characteristics of diverse land cover types can be strengthened through band math. The indices include Normalized Difference Vegetation Index (NDVI) [24], Normalized Difference Bare Soil Index (NDBaI) [25], Normalized Difference Built-up Index (NDBI) [26] and Normalized Difference Water Index (NDWI) [27] (Table A3). Third, height

Table 3

Summary of regression models quantifying the contribution of the area of different built types to SUHI extent during daytime and nighttime in summer and winter.

Season	Day/ Night	Regression model	R ²	Adjusted R ²
Summer	Daytime	$SUHI_{extent} = 12.828LCZ_1 + 3.021LCZ_6 + 1.392LCZ_3 + 554.102$	0.927	0.919
	Nighttime	$SUHI_{extent} = 5.061LCZ_1 + 2.282LCZ_6 + 1.972LCZ_3 + 294.118$	0.922	0.913
Winter	Daytime	$SUHI_{extent} = 13.836LCZ_1 + 2.757LCZ_6 + 1.305LCZ_3 + 279.767$	0.959	0.954
	Nighttime	$SUHI_{extent} = 4.105LCZ_1 + 2.668LCZ_6 + 1.628LCZ_3 + 0.993LCZ_4 + 258.529$	0.947	0.939

information was added to the input for the refinement of LCZ built types which have a relatively low classification accuracy when using the previous WUDAPT workflow. Digital Surface Model (DSM) and Digital Terrain Model (DTM) data were used to supplement the height information which Landsat images lack, including the ALOS global digital surface model (AW3D30) [28], the Shuttle Radar Topography Mission (SRTM) digital elevation data [29] and the Global Multi-resolution Terrain Elevation Data 2010 (GMTED2010) [30]. Moreover, the canopy height determined by subtracting the Digital Terrain Model (DTM) data from Digital Surface Model (DSM) data served as an input feature roughly representing the height of human settlements and natural landscape.

2.2.1.2. Sample datasets. Sample datasets play a critical role in generating LCZs [15]. The improved LCZ mapping method assesses

classification accuracy by dividing the complete sample datasets into training and validation sets. A training set was used to predict LCZs and validation sets were employed for accuracy assessment. Fig. 2 presents the workflow of selecting samples for LCZ classification. Following the general guidelines of sample selection for LCZs (<https://www.wudapt.org/digitize-training-areas/>), samples were digitized through visual interpretation and length/width measurement on high-resolution images in Google Earth Pro. To improve the quality of samples, we utilized Baidu Street View and housing agency websites (e.g., <https://www.fang.com/>) to supplement information on building function, building height, green coverage ratio, construction completed year and others. According to the geometric and surface cover properties determining LCZs obtained from Google Earth Pro, Baidu Street View and housing agency websites, one can easily identify the sample's LCZ type. Besides, the temporal consistency of training samples was also examined. Samples in the most recent year were collected first, then rechecked along the timeline to identify whether their LCZ types have changed. For those changed ones, their types will be reassigned or removed. This sample selection procedure was repeated for all years (Fig. A1).

2.2.2. Classification procedure

LCZ classification workflow in this study includes three main steps (Fig. 3): (1) processing earth observation data, (2) selecting samples for model training and validation, and (3) applying a random forest (RF) classifier. Step (1) and (3) were performed on the GEE platform and Step (2) was conducted using Google Earth Pro software.

First, earth observation data were processed using predefined functions of GEE, including removing cloud, clipping to the size of study areas and resampling data into a common-resolution grid. Second, training samples were digitized in KMZ or KML files, as described in Section 2.2.1 (2), and uploaded to GEE as input data for subsequent classification. Third, a RF classifier was used to classify LCZs due to its robustness, relatively high accuracy and computational performance [31]. The RF algorithm classifies every image pixel into one LCZ type using integrated decision trees [8]. Based on the samples collected in Step (2), this study used a random sampling strategy to generate training sets and validation sets. The training and validation set were randomly split as 7:3, and the split was repeated 25 times. 70% of the total samples were used to train the classifier and predict LCZ classes; the remaining 30% were used for accuracy assessment by comparing their “true” LCZ types with the predicted ones. After the three steps, an initial LCZ map was produced.

2.2.3. Post-classification processing and accuracy assessment

2.2.3.1. Temporal consistency check. Post-classification processing was conducted to check whether the generated historical LCZ maps are reasonable, according to the basic assumption that transformation from urban to natural types (including agricultural types) is unlikely to happen [32]. In this study, a temporal consistency check was implemented for the initial LCZ maps of each city in four years following these two rules:

Rule (1): For every time interval of five years, a pixel assigned as an LCZ built type is relatively stable, which means conversion from LCZ built type to natural type is uncommon. If a conversion from built type to natural type occurs, the LCZ natural type in the forthcoming year will be altered to built type in the current year.

Rule (2): LCZ high-rise types are unlikely to change to LCZ low-rise types (e.g., LCZ 4 is unlikely to transform to LCZ 3). The cost of demolishing high-rise buildings and reconstructing new buildings is quite large in Chinese megacities where land prices are usually high. Hence, pixels classified as LCZ 1 and LCZ 4 remain the same in the following year.

Based on these two rules, a temporal consistency check was performed for every pair of LCZ maps (2000 vs. 2005, 2005 vs. 2010 and 2010 vs. 2015).

2.2.3.2. Accuracy assessment. To assess the classification accuracy, a confusion matrix was calculated for each result by comparing the classified LCZ types with those established in the validation samples. The commonly used accuracy evaluation index, overall accuracy (OA), was applied in this study. To further specify accuracies of natural and built types, two additional indices of accuracy evaluation were employed. One is the overall accuracy of LCZ built types (OA_u), and the other is the overall accuracy of LCZ natural land covers (OA_n) [12].

$$OA = \sum_{i=1}^{17} N_i^{correct} / N_{total} \tag{1}$$

$$OA_u = \sum_{i=1}^{10} N_i^{correct,urban} / N_{total,urban} \tag{2}$$

$$OA_n = \sum_{i=11}^{17} N_i^{correct,natural} / N_{total,natural} \tag{3}$$

where

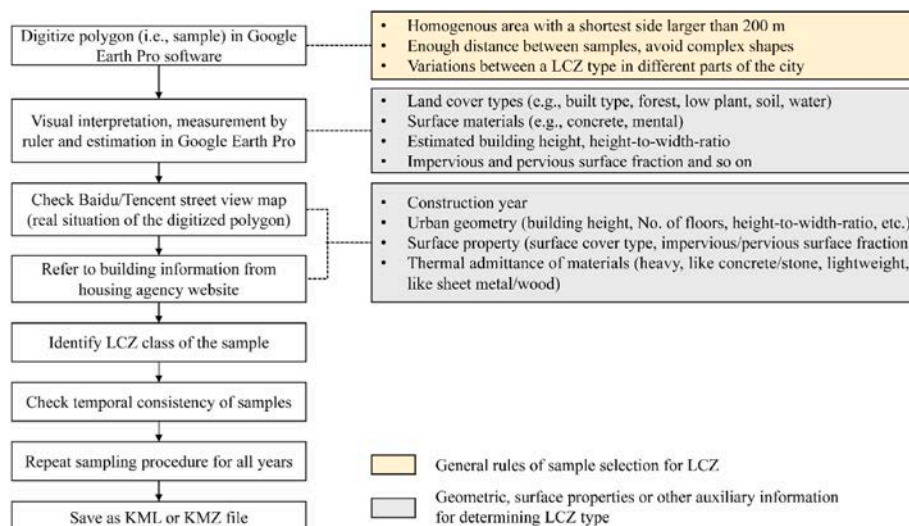


Fig. 2. Workflow of selecting samples for LCZ classification.

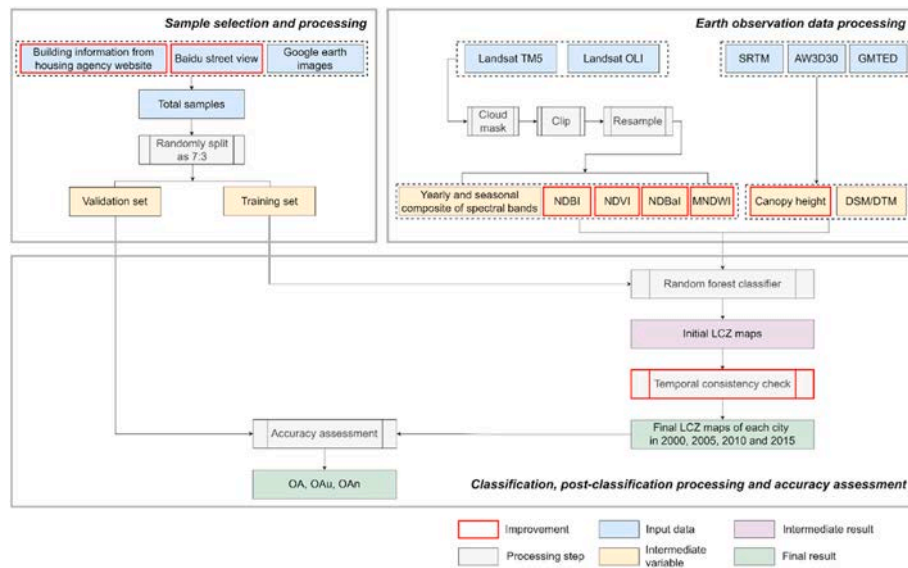


Fig. 3. General workflow of the improved LCZ mapping method.

N_{total} , $N_{total,urban}$ and $N_{total,natural}$ refer to the total number of ground truth for all classes, built types and natural land covers, respectively.

$N_i^{correct}$, $N_i^{correct,urban}$ and $N_i^{correct,natural}$ refer to the correctly classified pixels of all classes, built types and natural land covers, respectively.

2.3. Spatial-temporal patterns of the SUHI effect

2.3.1. Dataset

LST, which is usually used to quantify the SUHI effect, was derived from MODIS data product MOD11A2 Version 6 for each city in 2000, 2005, 2010 and 2015. MOD11A2 LST was acquired at 10:30 a.m. and 10:30 p.m. local time with a spatial resolution of 1 km. Each pixel value is the average of clear-sky LSTs over eight days. The LST was retrieved using a generalized split-window algorithm and further improved by correcting noise caused by topography, cloud contamination and zenith angle changes [33]. The error of MODIS LST data was reported to be lower than 1 K [33]. The advantages of broad coverage, high temporal resolution, long historical archive and high accuracy make MODIS LST data suitable for SUHI analysis across large cities.

DTM data with approximately 225-m resolution from GMTED2010 was used to reduce the impact of elevation on SUHI estimation. Overlaying DTM data with true-colour remote sensing images, the elevation range of mountains was identified through visual interpretation, and corresponding pixels were excluded. Water pixels and pixels with elevations ± 50 m off the average elevation of the urban core were also removed from the subsequent SUHI analysis [34]. LSTs were averaged over summer (1 June to 31 August) and winter months (1 December to 28/29 February).

Air temperature, precipitation and relative humidity records obtained from the China Meteorological Data Service Centre (<http://data.cma.cn/>) in 2000, 2005, 2010 and 2015 were used to represent the background climate of each city. Limited by data accessibility, the completeness of historical archives and surrounding settings (e.g., water, mountain) of the meteorological stations, records of 16 stations in total were collected.

2.3.2. Intra-urban SUHI intensity

The fine intra-urban classification of the LCZ scheme makes intra-urban SUHI investigation possible and makes an easy cross-comparison amongst cities with diverse geographic, climatic and socioeconomic (like population, economic development, and public fa-

cility) conditions. In this study, the SUHI intensity of the specific LCZ built type (i.e., the intra-urban SUHI intensity) was calculated during daytime and nighttime in summer and winter since significant health (e.g., respiratory disease, cardiovascular disease, increased morbidity among vulnerable people with physical or mental illness) and socioeconomic (e.g., energy consumption for heating or cooling, economic loss caused by reduced labor productivity during heatwaves) impacts of SUHI are reported in these two seasons [4,35–37]. Equation is as the following [38].

$$SUHI_{LCZ\ built\ type\ i} = \overline{T_{LCZ\ built\ type\ i}} - T_{rural} \quad (4)$$

where $SUHI_{LCZ\ built\ type\ i}$ refers to the heat island intensity of LCZ built type i , $T_{LCZ\ built\ type\ i}$ is the LST value of LCZ built type i , and T_{rural} is the mean LST of rural reference (LCZ D).

2.3.3. SUHI extent

Apart from the magnitude of the SUHI effect, the spatial extent was also explored for every large city at day and night in summer and winter. In this study, the SUHI extent was defined as the areas with a significant increase in SUHI intensity compared with rural areas. That is, the SUHI intensity reduces gradually from the dense urban center to the urban fringe and then decreases significantly between urban edges and rural areas. A “break point” is assumed to exist in the urban-rural transition zone where the SUHI effect changes from large magnitude to small magnitude. Such a “break point” can be used to identify the spatial extent of the SUHI effect.

Fig. 4 shows an example calculating the SUHI extent of Shanghai during the summer daytime. The main urban area was first identified by merging LCZ built types, and the urban border was depicted correspondingly. Then, buffers with a 250-m distance were generated inwards and outwards from the urban border until the inner urban areas and the rural areas within the administrative boundary of the city were filled, respectively. According to the sensitivity test, the value of SUHI extent is stable under a buffer distance of 250 m (Table A4). Due to the high correlation between LST and human settlements, the central buffer was taken as the starting buffer for SUHI extent identification. Finally, the mean SUHI intensity of each buffer was computed, and the relationship between the number of buffers and averaged SUHI intensity was plotted. Then, a piecewise regression model was implemented to find the “break point” which separates the area with and without significant SUHI effect using

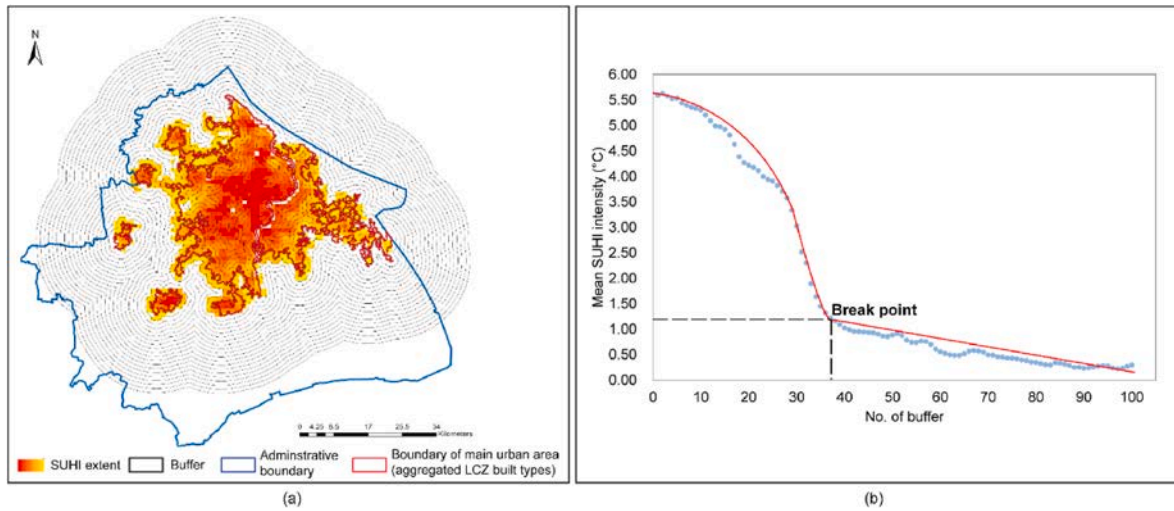


Fig. 4. Illustration of calculating the SUHI extent in Shanghai in summer daytime of 2000 (1 June–31 August). The example of (a) SUHI extent with SUHI intensity higher than 1.22 °C (area with warm colors), main urban area aggregated from LCZ built types (red line), buffers (light grey area), and the administrative boundary of the city (dark blue line); (b) piecewise regression line between buffer No. and mean SUHI intensity to identify “break point”. (For interpretation of the references to colour in this figure legend, the reader is referred to the Web version of this article.)

$$SUHI\ intensity = \begin{cases} f_1(x), & |x < x_{breaking\ point} \\ f_2(x), & |x \geq x_{breaking\ point} \end{cases} \quad (5)$$

where $x_{breaking\ point}$ is the x coordinate (buffer number) of the break point, $f_1(x)$ and $f_2(x)$ refer to two regression functions that describe the relationship between mean SUHI intensity and buffer numbers. The functions can either be linear, logarithmic, polynomial or other forms.

Lastly, the averaged SUHI intensity at the break point was identified as the minimum value for the significant SUHI effect. Areas with SUHI intensity higher than the minimum value were identified as SUHI extent.

2.3.4. Correlation analysis

A Pearson’s correlation analysis was applied to investigate the impact of background climate on the SUHI effect. First, the annual seasonal mean air temperature, relative humidity and precipitation of

each city were calculated. Second, Pearson’s correlation coefficients were used to examine the strength of the relationship between (1) intra-urban SUHI intensity and background climate and (2) SUHI extent and background climate across selected large Chinese cities during both daytime and nighttime in summer and winter.

3. Results

3.1. LCZ maps

Following the GEE-based LCZ mapping method, the LCZ maps of selected Chinese cities were generated in 2000, 2005, 2010 and 2015. Fig. 5 shows the overall accuracies of all LCZ classes, LCZ built types and LCZ natural types. Generally, the overall accuracies of 17 LCZ classes for these cities range from 80.92% to 93.91%, with a mean value of 88.14%

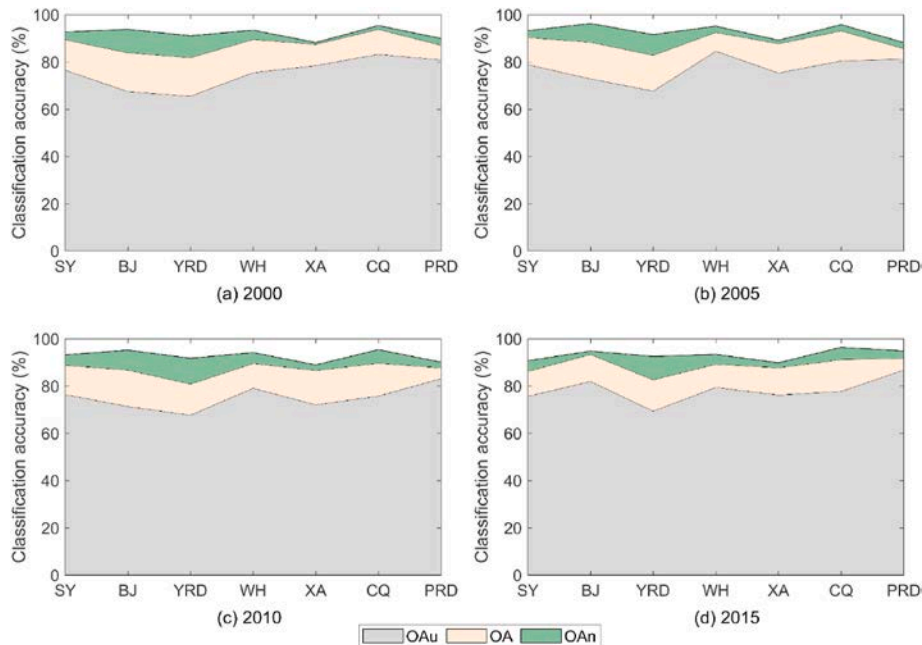


Fig. 5. Accuracy assessment results of large cities in (a) 2000, (b) 2005, (c) 2010, and (d) 2015 (OA: overall accuracy of all classes, OAu: overall accuracy of built types, OAn: overall accuracy of natural types).

and a standard deviation (SD) of 3.42%. For all study targets, the overall accuracy of natural types performs considerably better than that for built kinds. The averaged overall accuracy of the natural types achieves 92.72%, with a SD of 2.49%. However, the overall accuracy of the built types ranges from 65.69% to 86.85%; the mean value of built types is 76.54% and SD is 5.50% (Table A5).

Fig. 6 presents the LCZ maps of each large city in 2000, 2005, 2010 and 2015. All 17 LCZ types can be found in most of these cities, although

LCZ 1 (compact high-rise) and LCZ 4 (open high-rise) were not detected in the early stage of urban development for several cities. For example, Xi'an lacked LCZ 1 in 2000, and Shenyang lacked LCZ 1 and LCZ 4 in 2000. Evidently, the proportion of natural land cover area continuously decreased for all study targets from 2000 to 2015. However, the area of the built types continuously increased for all large Chinese cities from 2000 to 2015 (Fig. 6).

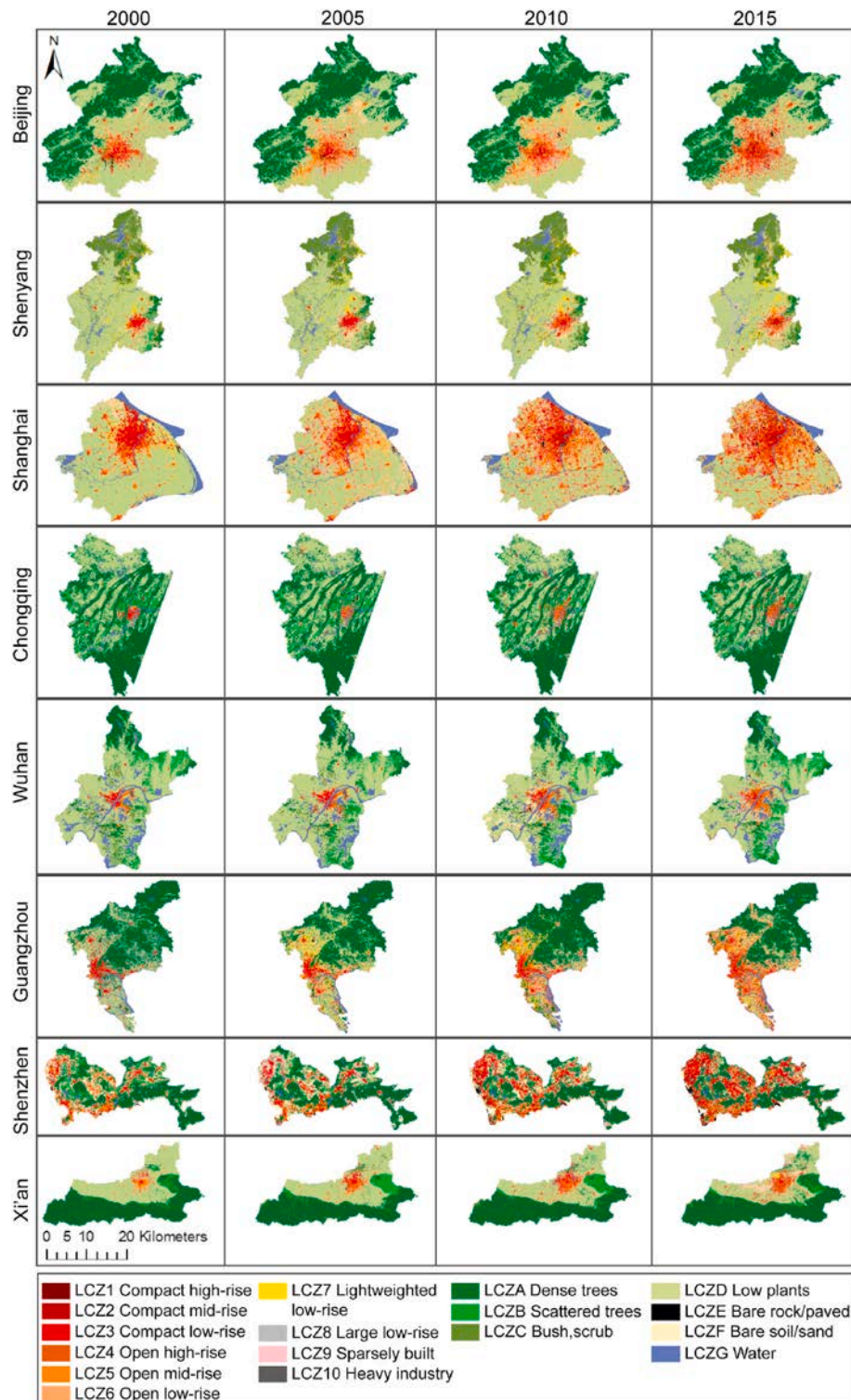


Fig. 6. LCZ maps of eight large cities in China in 2000, 2005, 2010 and 2015.

3.2. Spatial-temporal patterns of SUHI intensity

An important advantage of the LCZ classification scheme is that it classifies the general urban classes into ten specific built types according to their building height, spatial arrangement (compact/open) and thermal properties. The specific built types make it possible to investigate the intra-urban SUHI intensity in cities, which is closely related to human activities. Further urban heat island mitigation measures can thus be proposed based on the intra-urban SUHI variations. Fig. 7 shows the four-year-averaged SUHI intensities of each LCZ built type for eight large cities during the daytime and nighttime of summer and winter. Fig. A2 further displays boxplots of the intra-urban SUHI intensity in each large city during daytime and nighttime in winter and summer from 2000 to 2015. Fig. 8 illustrates the spatially changing trend of the intra-urban SUHI intensities.

3.2.1. Temporal patterns

The intra-urban SUHI intensities present a significant seasonal pattern. During winter days, the SUHI effect is not well developed in large cities; it is usually below 2 °C (Fig. A2). For cities in severe cold or cold regions, the highest SUHI intensities are in low-rise types with a large area of impervious surface (i.e., LCZ 8 and LCZ 10) (Fig. 7 (c)). In terms of cities located in regions with hot summer and cold winter, compact LCZ type and openly arranged low-rise settlements (LCZ 8 or LCZ 10) exhibit the highest SUHI intensity (Fig. 7 (c)). For cities located in regions with hot summer and warm winter, like Guangzhou and Shenzhen, the hottest LCZ built types are LCZ 2, LCZ 3 and LCZ 8 (Fig. 7 (c)).

During winter nights, SUHI intensities of most built types are higher than that in winter days (Fig. 7 (c) and (d)). For cities in severe cold or cold regions, LCZ 1, LCZ 2 and LCZ 4 are normally the warmest built types (Fig. 7 (d)). For cities in regions with hot summer and cold or warm winter, the warmest built types are usually LCZ 1 and LCZ 2 (Fig. 7 (d)).

Intra-urban SUHI intensities achieve their highest values for the majority of the eight large cities during summer days (Fig. 7 (a)). The hottest built types in summer days for all large cities are LCZ 1 and LCZ 2, followed by LCZ 4 or LCZ 8, except for Guangzhou and Shenzhen (Fig. 7 (a)). In those cities, LCZ 2 and LCZ 3 are the top two warmest built types (Fig. 7 (a)).

Summer-nighttime SUHI intensity of every built type is commonly the second-highest in the eight cities, except for those with a relatively cold climate (such as Shenyang) (Fig. 7 (b)). In Shenyang, the SUHI intensities of LCZ 1, 2 and 4 in winter nights are even higher than those in summer days (Fig. 7 (b)). The hottest built types in most cities are still LCZ 1 and LCZ 2 during summer nights (Fig. 7 (b)).

The coolest built types across seasons, times and climate zones are usually LCZ 7 and LCZ 9 (Fig. 7 (a)–(d)). SUHI intensities of both types achieve their highest and lowest values in summer days and winter days, respectively.

3.2.2. Spatial patterns

The intra-urban SUHI intensities show an apparent spatial pattern during summer days, summer nights and winter nights (Fig. 8). The SUHI intensity generally reduces with increasing air temperature, precipitation and relative humidity. The intra-urban SUHI intensity is

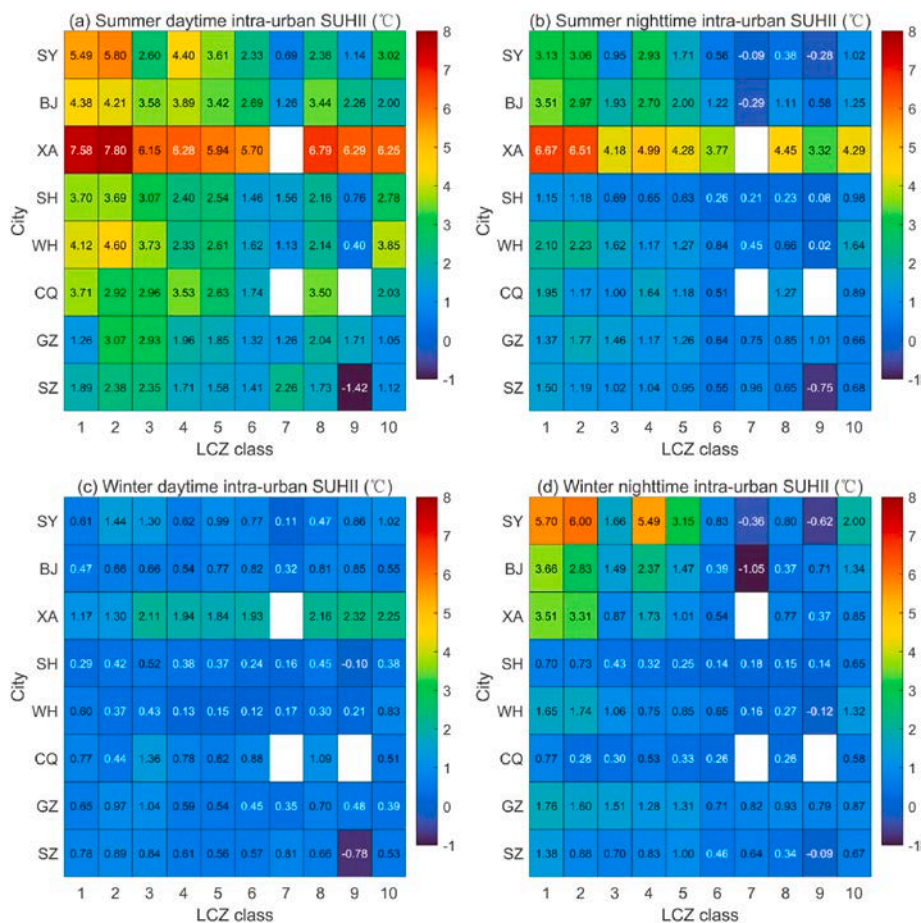


Fig. 7. Mean SUHI intensities of each built type for all eight large cities in summer daytime, summer nighttime, winter daytime and winter nighttime for all four years studied (2000, 2005, 2010, 2015). Red colors indicate higher SUHI intensities; blue colors indicate lower SUHI intensities. Blank cells indicate that LCZ type is not detected in the respective city. (For interpretation of the references to colour in this figure legend, the reader is referred to the Web version of this article.)

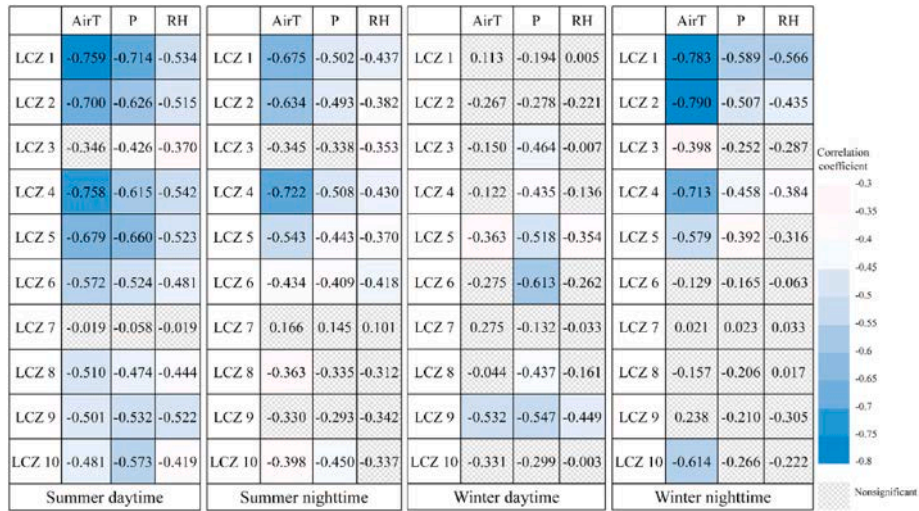


Fig. 8. Correlation coefficients between intra-urban SUHI intensities and background climate (annual mean air temperature-AirT, precipitation-P and relative humidity-RH in summer and winter).

noticeably higher in cities in severe cold or cold regions compared to those in regions with hot summer and cold/warm winter (Figs. 7 and 8).

During winter days, the spatially decreasing pattern of the intra-urban SUHI intensities from the north (severe cold region) to the southeast (region with hot summer and warm winter) of China is least apparent. Only weak and moderate correlations are found between SUHI intensities and background climate. Besides, only the SUHI intensities of LCZ 5 and LCZ 9 are significantly negatively correlated to all the three meteorological indicators.

During winter nights, according to the correlation coefficients shown in Fig. 8, a significant decreasing trend of the SUHI intensity from a cold and dry climate to a warm and wet climate is observed in LCZ 1, LCZ 2 and LCZ 4. The SUHI intensity of built types can reach as high as 6.00 °C (LCZ 2 in Shenyang) in a severe cold region, with LCZ 1, 2 and 4 presenting the highest SUHI intensities. Compared to severe cold regions, SUHI intensities of the warmest built types (LCZ 1, LCZ 2 and LCZ 4) in cold regions decrease—3.66 °C (LCZ 1, Beijing), 2.83 °C (LCZ 2, Beijing), 2.37 °C (LCZ 4, Beijing), 3.51 °C (LCZ 1, Xi'an), 3.31 °C (LCZ 2, Xi'an) and 1.73 °C (LCZ 4, Xi'an). For cities in regions with hot summer and cold or warm winter, SUHI intensities of the warmest built types continually drop.

During summer days, the negative correlation between intra-urban SUHI intensities and background climate is the strongest. Negative correlations between SUHI intensities of most LCZ built types and background climate are found. Among the ten built types, the SUHI intensity of LCZ 1 shows the most apparent spatial pattern, according to its largest absolute value of correlation coefficient ($r_{\text{airT-LCZ 1}}$: 0.759, $r_{\text{P-LCZ 1}}$: 0.714, $r_{\text{RH-LCZ 1}}$: 0.534). The SUHI intensity of LCZ 1 achieves the highest value (7.58 °C) in Xi'an, followed by Shenyang (5.49 °C) and Beijing (4.38 °C) which are all located in severe cold or cold regions. Cities in regions with hot summer and cold winter show slightly lower SUHI intensity of LCZ 1, with 4.12 °C in Wuhan, 3.71 °C in Chongqing and 3.70 °C in Shanghai. The hottest built type in Guangzhou and Shenzhen, with relatively warm and wet climates, shows the lowest SUHI intensity amongst the eight large cities, with a mean of 3.07 °C and 2.38 °C, respectively.

During summer nights, such a spatially decreasing pattern of intra-urban SUHI intensities from the northern to the southeastern region of China is stronger than during winter days but weaker than those during summer days and winter nights. However, the number of built types showing a significant negative correlation between their SUHI intensities and the three meteorological indicators is the second-largest in summer nights—eight during summer days, five during summer nights,

two during winter days and three during winter nights.

3.3. Spatial-temporal patterns of SUHI extent

Apart from discussing the traditional SUHI-related index—SUHI intensity, this study also put forward a buffer-based approach to map the spatial extent of significant SUHIs. Following the method presented in Section 2.3.3, the average SUHI intensity of each buffer zone for each large city in summer and winter was calculated from 2000 to 2015. Taking Shanghai as an example, the mean SUHI intensity in buffers decreases gradually, as shown in Fig. 9. The mean SUHI intensity in the central buffer is significantly larger than in other buffers. With the buffers continuously expanding, the average SUHI intensity decreases, and after a certain point, the downward trend eventually slows. This point is the “break point” that separates the city area with significant SUHIs (i.e., SUHI extent) from that without significant SUHIs. According to the piecewise regression model, buffer No. 37 (1.22 °C), No. 36 (0.26 °C), No. 35 (0.22 °C) and No. 28 (0.35 °C) are taken as the break points during summer days, summer nights, winter days and winter nights in 2000, and corresponding SUHI extent can be extracted.

3.3.1. Temporal patterns

Fig. 10 shows the absolute and normalized SUHI extent of every city separated by season and day/night. Fig. A3 further maps the spatial distribution of the significant SUHI effect for each city during summer and winter from 2000 to 2015.

From a seasonal perspective, the most significant SUHI extent is observed in summer daytime for all large cities (Fig. 10). From 2000 to 2015, Beijing had the largest absolute and normalized SUHI extent with a four-year average of 3877.5 km² and 2.34 times of the main urban area, respectively, during summer daytime (Fig. 10 (a) and (e)). Large cities exhibit the second-largest SUHI extent during summer nighttime, and Beijing also has the widest SUHI influencing area (Fig. 10 (c) and (g)). The difference between daytime and nighttime SUHI extent is most significant in summer (Fig. 10). Wintertime SUHI extent is smallest for all the eight large cities (Fig. 10 (b), (d), (f), (h)). The corresponding day-night difference is normally smaller than that in summer.

From a time-series perspective, SUHI extents in the eight large cities follow a rising trend regardless of daytime/nighttime, seasons and geographical or climatic conditions (Fig. 10 (a)–(d)). However, in terms of the annual growth rate of SUHI extent, all the eight large cities do not display a continuous trend across all times (day/night) and two seasons (summer/winter), except for Xi'an, with a continuous decreasing trend

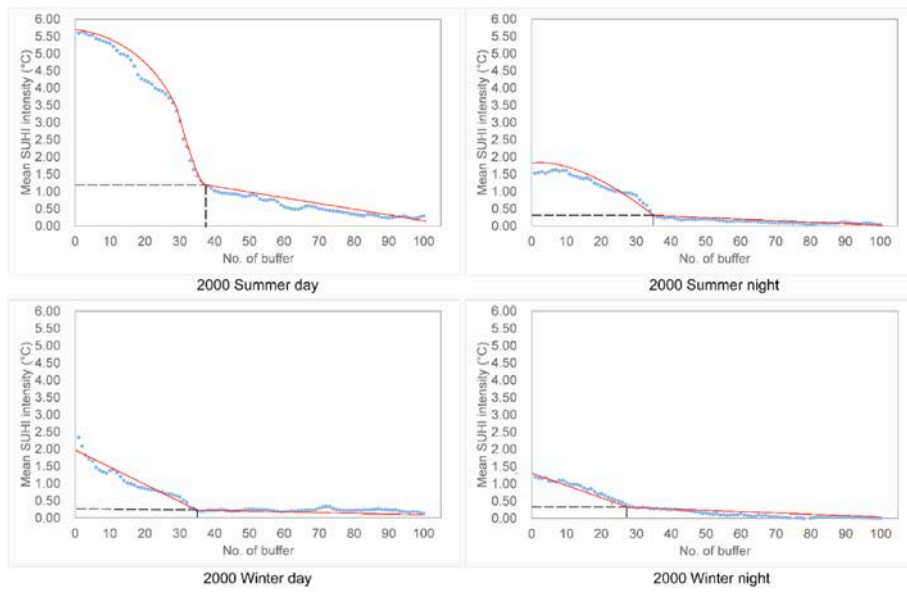
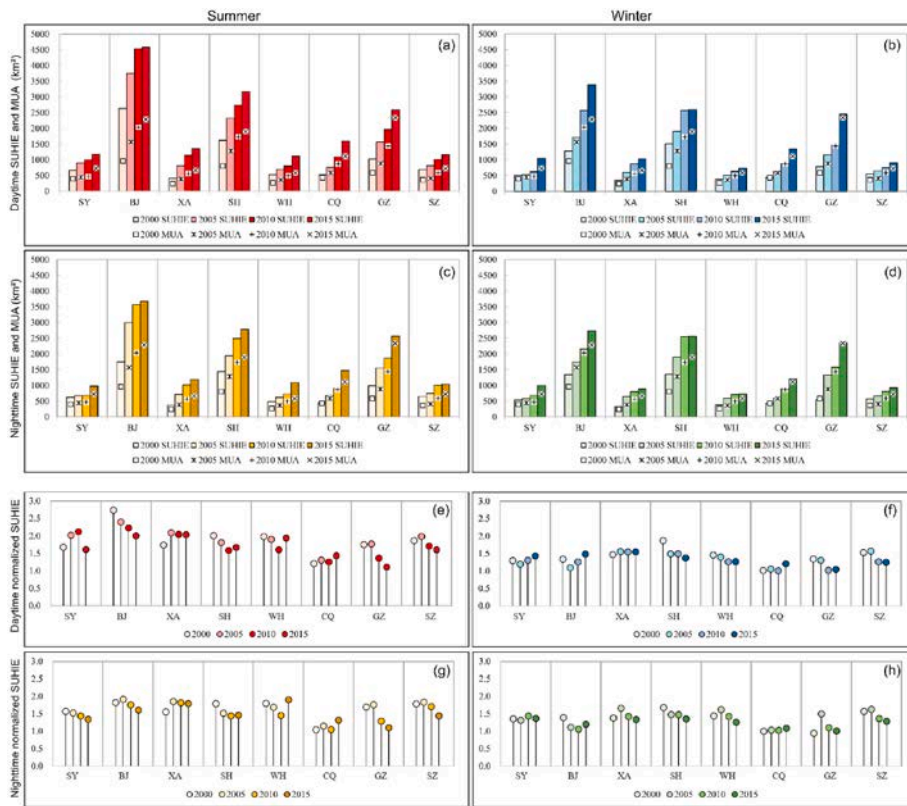


Fig. 9. The “break point” in Shanghai during daytime and nighttime in summer and winter in 2000. Intersections of black dash lines refer to the “break point”. The red line indicates the regression model before and after the “break point”. (For interpretation of the references to colour in this figure legend, the reader is referred to the Web version of this article.)



Note: SY—Shenyang, BJ—Beijing, XA—Xi’an, SH—Shanghai, WH—Wuhan, CQ—Chongqing, GZ—Guangzhou, SZ—Shenzhen.

Fig. 10. Absolute (a–d) and normalized (e–h) SUHI extent (SUHIE) of each large city during daytime and nighttime of summer and winter in 2000, 2005, 2010 and 2015. The main urban area (MUA) in every city in the four years is also shown.

(Fig. 11). Although the SUHI extents in both Beijing and Shanghai expand during summer, their annual growth rates gradually drop, illustrating a slowing of SUHI expansion in both cities (Fig. 11 (a) and

(c)). Besides, most cities have larger annual growth rates of main urban areas than those of SUHI extents, indicating that urban areas of large cities grow faster than SUHI extents (Fig. 11).

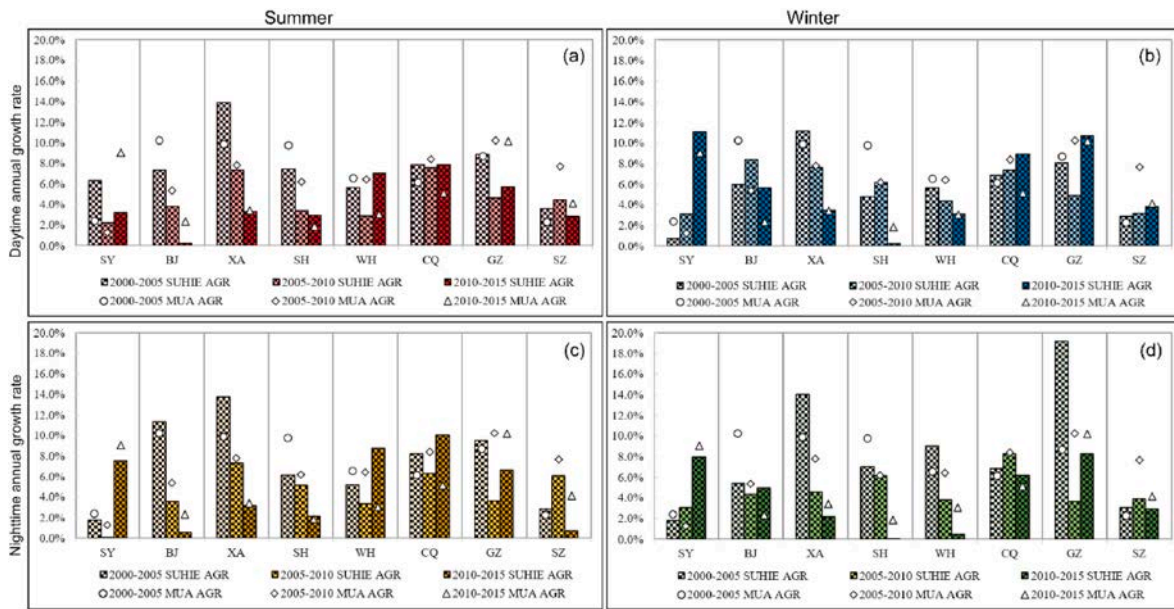


Fig. 11. Annual growth rate of SUHI extent (SUHIE AGR) and main urban area (MUA AGR) for each large city during daytime and nighttime in winter and summer in three periods. The annual growth rate (AGR) is calculated as $AGR = \sqrt[n]{Area_{end}/Area_{start}} - 1$ (n : No. of years, $Area_{start}$: area of the starting year, $Area_{end}$: area of the ending year) [39].

3.3.2. Spatial patterns

From a spatial perspective, cities with a dry climate and a broad urban area tend to have a larger SUHI extent than those with a wet climate and less urban area. According to Table 2, there is no statistically significant correlation between air temperature, precipitation and SUHI extent since the corresponding p values are all larger than 0.05. However, a weak negative correlation was found between relative humidity and SUHI extent during the daytime, with p values smaller than 0.05. Taking the cities with the top-three largest SUHI extent as an example, the relative humidity of Beijing, Shanghai and Guangzhou increase (Table A2) while their SUHI extents decrease (Fig. 10). Besides, SUHI extent is found to be significantly related to the physical structure of a city, such as the total area of LCZ 1–10 (Table 2); such a correlation is stronger than that between SUHI extent and background climate. The SUHI extent is positively associated with the urban area during both daytime and nighttime of summer and winter. Such a correlation achieves its highest value during summer daytime with a correlation coefficient of 0.9. More heat absorption due to large areas of impervious surfaces and more heat emissions from human activities drive higher urban heat in large cities than in medium or small cities.

3.4. Relationship between LCZ built types and SUHI effect

The application of the LCZ scheme makes it possible to investigate intra-urban differences in the thermal environment. The findings of this study confirmed that the intra-urban SUHI intensity varies across time and space, which is consistent with others' work [1,11,38,40]. Although the specific LCZ built type with the highest SUHI intensity is sensitive to seasons, times (day and night) and climate zones, it usually belongs to compact built types, like LCZ 1 and LCZ 2, or large low-rise types (LCZ 8). Additionally, LCZ 1 is also positively correlated to SUHI expansion in most cases. A multivariate linear regression model was built between the area of different built types and SUHI extent in large cities with a significance level of 0.05 (Table 3). The results show that not all built types are correlated to the changes in SUHI extent. Only three to four built types can significantly explain the variations in SUHI extent. Among them, LCZ 1 is the most influential built type of SUHI extent, regardless of times and seasons.

The reason that LCZ 1 presents high SUHI intensity and correlates to

a large SUHI extent is because of its highly complex urban morphology. In large Chinese cities, LCZ 1 is normally either high-rise and high-density buildings gathered in the Central Business District or residential buildings with a high plot ratio. The building geometry (e.g., low SVF, high height-to-width ratio) and surface properties (e.g., low urban greenery ratio, a large fraction of impervious surface) of LCZ 1 increase net energy input and decrease net energy output. The former mainly comes from increased net shortwave radiation absorbed by building surfaces during daytime and increased downward longwave radiation emitted by multi-facets during nighttime. The latter usually stems from less sensible heat flux caused by weakened air ventilation, less latent heat flux caused by little vegetation, and a reduced rate of longwave loss at night due to decreased SVF.

4. Discussion

4.1. Advantages of the improved LCZ mapping method

Compared to other existing LCZ classification methods, the newly proposed LCZ mapping method made improvements in several aspects (Fig. 3): (1) referring to Baidu Street View and housing agency websites to help identify LCZ types of training samples, (2) implementing several spectral indices to separate different land covers, (3) combining height information to refine the intra-urban LCZ classes' differentiation and (4) applying a temporal consistency check to ensure consistency of LCZ classes between different years. In summary, it has the following advantages:

First, this method generates markedly accurate LCZ classes in a complex urban context. The classification accuracies of all classes, natural land covers and built types produced by the improved LCZ mapping method increased by 6.87%, 6.04% and 9.79%, respectively, compared with the initial WUDAPT workflow (Fig. 12). The improvement in LCZ built types' accuracy is the highest.

Second, a temporal consistency check reduces the inconsistency of LCZ classes along a timeline. Most previous LCZ mapping studies focused on LCZ classification in a single year [10,41] or adjacent years [12]. Wang et al. [17] developed time-series LCZ maps of the PRD region in 1999, 2009 and 2014. A manual correction was conducted to ensure consistency amongst LCZ maps in discrete years. However, a manual

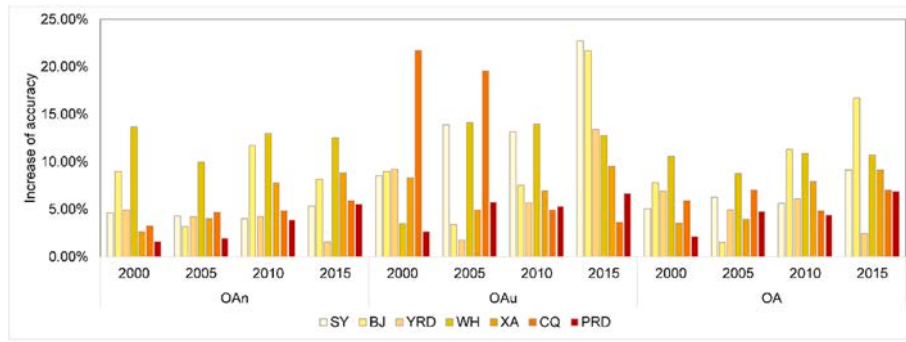


Fig. 12. Increase in classification accuracy of all LCZ types (OA), built types (OAu), and natural types (OAn) in eight large cities from 2000 to 2015, comparing the LCZ classification results generated by the original WUDAPT method with that produced by the improved LCZ mapping method.

correction is time and labor-consuming and has the probability of missing inconsistent pixels during a visual check. Through coding in MATLAB, the improved LCZ mapping method applied two rules (as shown in Section 2.2.3) to ensure temporally consistent LCZs amongst different years. This consistency reduces the probability of proposing inaccurate planning recommendations during subsequent urban planning practice.

Third, owing to the numerous geospatial datasets and remarkable computational speed of GEE, updating and managing LCZ maps is easy and convenient. Ease-to-update and management are particularly beneficial for developing countries that remain under rapid urbanization. Compared to a mean of 80% in developed countries, China still has room to improve its urban population ratio (60.6% in 2019) [5,6]. Hence, the LCZ maps of Chinese cities will require periodic updates to meet their needs arising from further urbanization and address the related urban environmental issues that affect human health and comfortable living.

4.2. Advantages of the buffer-based approach to measuring SUHI extent

Following the calculation method of a Gaussian surface described in Streutker [21], the spatial extent of the SUHI effect in Shanghai during the summer day of 2000 was extracted, as shown in Fig. 13. The SUHI footprint generated through the Gaussian surface model is represented

by an ellipse with a short semi-axis of 21.68 km and a long-semi axis of 28.75 km. Generally, the SUHI extents generated by the Gaussian surface method and buffer-based approach are highly consistent, with an overlapping ratio of 85.14%. Comparing the SUHI extent generated by both methods, the one produced by the Gaussian surface model has a larger area (1958 km²) than that detected by using the buffer-based approach (1667 km²). However, the Gaussian surface model cannot generate an accurate spatial extent of the SUHI, but only a simple ellipse that even misses the isolated hot spots in Songjiang and Qingpu District (Fig. 13).

The buffer-based approach has two important advantages. First, this approach can capture the spatial extent of the SUHI effect in cities with multi-core urban development modes. Limited by its mathematical origins that the Gaussian surface must be continuously closed, the Gaussian surface is only suitable to describe single-core SUHI extent. However, multi-core urban planning is much more common in recent planning policies [18]. Second, the buffer-based approach can produce a more accurate spatial extent of the SUHI, which is consistent with the urban planning reality. This is because that buffers are the boundaries of aggregated LCZ built types in different sizes but the same shape, depicting the on-the-ground reality. Compared to the buffer-based approach, the Gaussian surface only provides a simplified ellipse that includes not only the areas affected by the SUHI but also those with low surface temperatures that should be excluded [2,18]. Besides, some

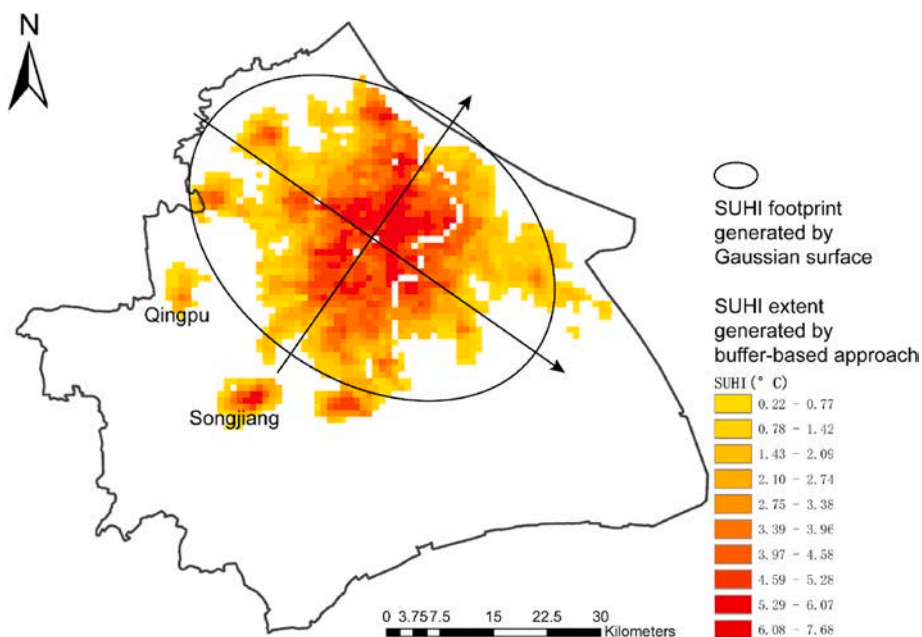


Fig. 13. SUHI extent generated by Gaussian surface model (the ellipse) and buffer-based approach (area with colors) in Shanghai during the summer day in 2000.

scholars tried a logistic model to determine the SUHI extent by calculating the decreasing trend of LST from urban to rural areas [42]. But this method generates a spatial probability of the SUHI rather than an exact SUHI extent which can serve as a spatial decision reference for planning practice.

However, the proposed calculation method of SUHI extent is less automated in finding break points since users need to make a scatter plot of “buffer No.—SUHI intensity” first and find the respective fitting function for each piece. It may increase time cost when calculating SUHI extent at a large scale and for multiple years.

4.3. Potential factors associated with the spatial-temporal patterns of the SUHI

4.3.1. Background climate

Background climate is one major factor influencing the spatial-temporal variation of the SUHI. Our results show that the intensity and extent of the SUHI tend to decrease with climates becoming warm and humid, which is consistent with previous work [43–46]. Climate affects SUHI mainly by changing the properties of rural reference (like moisture). Compared to dry surfaces, wet or saturated soil absorbs more solar radiation while slowing down its heating or cooling rate, resulting in a smaller daily temperature range [44]. The weakening impact of humidity on the SUHI can also be explained by the suppressed evaporative cooling of rural surfaces when the atmospheric water vapor pressure is high, resulting in a decreased urban-rural temperature difference [47]. Hence cities located in the southeast region of China (wet climates) have a smaller SUHI intensity and SUHI extent than those in the northern areas (dry climates).

4.3.2. Vegetation activities

The presence of vegetation correlates negatively to SUHI as it has a cooling effect on LST via transpiration [45]. Seasonal changes in vegetation activities largely contribute to the spatial-temporal pattern of heat islands. Evapotranspiration of vegetation is more active in summer compared to other seasons since vegetation is the most flourishing [45]. Rural areas covered by abundant greenery have relatively strong evapotranspiration during summer, leading to a more considerable urban-rural temperature difference than in other seasons. Thus, both SUHII and SUHIE present the highest value on summer days but a relatively low value in winter. This finding agrees with previous studies [1,2].

4.3.3. Surface albedo

Surface albedo is an important influencing factor for the spatial variability of nighttime SUHI across different climate zones [40,45]. Impervious surfaces usually have low surface albedo, increasing net all-wave radiation and heat storage in urban areas compared to rural areas covered by pervious surfaces [48]. Because nighttime SUHI is driven by surface heat fluxes stemming from daytime heat storage [49], cities with a larger negative difference in urban-rural albedo tend to have higher SUHI intensity at night. Such a correlation between SUHI intensity and albedo has been confirmed by previous work [40,45]. SUHI extent is negatively correlated to albedo because materials with low albedo attain higher LST when exposed to the sun [2].

Seasonal changes of albedo across different climate zones are closely associated with the spatial-temporal patterns of the SUHI. Cities surrounded by cropland and deciduous vegetation present a higher urban-rural albedo difference than those covered by evergreen forests [48]. Hence, northeastern cities with cold climates (like Shenyang and Beijing) characterized by seasonal low plants (i.e., LCZ D, including crop, grass, herbaceous plants) and deciduous trees exhibit high SUHI intensity during nighttime. Conversely, southeastern cities with warm climates (like Guangzhou and Shenzhen) covered by continuous low plants and evergreen trees have low nighttime SUHI intensity. Additionally, seasonal changes in surface albedo also contribute to the

temporal pattern of the SUHI. In agreement with Zhou et al. [45], our work indicates that cities with cold climates present higher SUHI intensity during winter nighttime compared to summer nighttime. This can be partially explained by a greater urban-rural albedo difference caused by ice and snow and vegetation defoliation in winter.

4.3.4. Urban area

As reported in this study and other work, the total area of impervious surface in a city (i.e., urban area) positively correlates to the intensity and extent of SUHIs [43,46]. Large areas of impervious surfaces absorb more heat and raise urban temperatures. Besides, a larger urban area usually means more urban population and higher anthropogenic heat emissions, which expands the temperature gap between urban and rural areas and intensifies the SUHI.

4.3.5. Anthropogenic heat

Anthropogenic heat release is reported to intensify SUHIs, particularly at night [45]. Besides heat storage during the day, anthropogenic heat produced by the city also serves as one of the energy fluxes driving nighttime SUHI [40]. Scholars commonly used remotely sensed nighttime light (NL) data as a proxy for anthropogenic heat release and found a positive relationship between urban-rural NL contrast and SUHI intensity [40,45]. A positive correlation between SUHI extent and NL was also reported, signifying more human activities may induce a broader extent of SUHIs [2].

Additionally, anthropogenic heat discharge contributes to the spatial variability of SUHI intensity across climate zones during winter nighttime. Our study found that SUHIs in northern China are more significant than in southern regions during winter nighttime, in agreement with other studies [45]. This is because cities in northern China are provided with central heating in winter, increasing anthropogenic heat emissions in urban areas compared to rural areas.

The mechanism underlying spatial-temporal patterns of SUHII and SUHIE is complicated. In addition to the factors discussed above, scholars reported that other factors associated with urban development could affect SUHI, such as urban form, air pollution, industrial structure and landscape configuration [50,51]. Overall, a combination of multiple factors leads to spatial-temporal variability of heat islands.

4.4. Implications for urban heat mitigation

The findings of this study have important implications for mitigating urban heat and creating a comfortable built environment for urban dwellers. Fig. 7 shows that LCZ 1 and LCZ 2 present relatively high daytime and nighttime SUHI intensity for the majority of large cities in China during both winter and summer. To mitigate the urban heat, planners should pay much attention to LCZ 1 and LCZ 2. Considering the large building coverage ratio (40%–70%) of compact types and the high cost of rearranging buildings, surface retrofitting with high-albedo materials and proper layout of blue-green infrastructure should be a feasible heat mitigation strategy. Besides, LCZ 4 (open high-rise) has lower SUHI intensity than LCZ 1 and LCZ 2. The ability to accommodate a similar population with compact high-rise/mid-rise buildings makes LCZ 4 a suitable building type for urban heat mitigation, balancing both space utilization and the need for building a comfortable living environment. Other studies also confirmed the relatively high SUHI intensity/LST in compact LCZ built types (e.g., LCZ 1–2) and large low-rise (LCZ 8) compared to open built types [9,38,52]. The air UHI intensities of LCZ 1 and LCZ 2 are stronger during nighttime than daytime [52–54]. Similar results to other studies assessing the “LCZ-UHI” relationship confirmed the necessity of controlling areas of compact types.

This study reveals the increasing trend of SUHI extent in large Chinese cities, causing more people to be exposed to heat islands. SUHI extent is positively correlated to the urban area (Table 2). Urbanization is expected to continue for another 20–30 years in China [55], accompanied by land cover transformation from natural types to artificial

impervious surfaces. Hence it is necessary to reduce the SUHI extent or at least restrain its expansion. Given the quantitative relationship between specific LCZ built type and SUHI extent (Table 3), developing extensive LCZ 1, 3 and 6 should be avoided in design and planning practice. Although LCZ 4 has the advantage over LCZ 1 and LCZ 2 in mitigating SUHI intensity, it can contribute to SUHI expansion during winter nighttime. A winter-nighttime SUHI expansion may be favorable for cities located in severe cold regions due to saving energy consumption for heating, but may not for cities in subtropical regions [56]. Hence, the area of LCZ 4 should be carefully assigned to achieve a balance between SUHI intensity and extent. Additionally, as shown in Table 2, a large continuous impervious surface area results in broad SUHI extent. In design or planning practice, it is suggested to avoid developing extensive impervious surfaces and try arranging buildings in a relatively dispersed way to restrain SUHI expansion.

Results proved that SUHI intensities and extents decline with climates becoming wet. Cities with dry climates should pay more attention to heat challenges, particularly in summer. Nevertheless, cities with low SUHI intensities under wet climates may also need heat mitigation when the absolute temperatures of urban areas are high in summer [56], like Guangzhou and Shenzhen. Uncomfortable urban temperatures bring heat-related problems, like a lack of thermal comfort, high energy consumption and human health issues.

Two considerations should be noted when adopting heat mitigation recommendations proposed in this study. First, SUHI is only one aspect of urban heat mitigation. SUHI does not examine air temperature directly, which is closely related to human health and thermal comfort. Besides, limited by the field of view of satellites, SUHI only considers a subset of the full urban surface. Second, the urban environment includes not only the thermal environment which can be represented by SUHI but also the air quality, carbon emissions, water quality and so on. The impact of heat mitigation measures on other aspects of the urban environment should also be considered.

4.5. Limitations and future studies

The LCZ-based SUHI analysis shown in this study can be transferred to a national scale or even a global scale in the future, subject to the availability of LCZ data and surface temperature. Although such a methodology can detect intra-urban thermal variation and the spatial extent undergoing significant heat islands, some limitations remain.

First, although LST has been shown to affect human health [4], the measurement of LST by remote sensing platforms does not sample all of the relevant surfaces (e.g., walls) that contribute to the heat exposure of urban residents outdoors or to the heat loading on buildings that can drive energy demand for cooling [52]. Second, due to limited freely available meteorological data, the impact of global climate change (e.g., increasing air temperature) on the SUHI hasn't been extracted. Third, only eight large cities located in different climate zones were selected in this study, and the analysis of the impact of climate on the LCZ-SUHI relationship should be refined. Last but not least, only potential major driving factors of the SUHI were discussed. The complicated mechanism and more driving factors remain to be further explored.

Future studies can (1) undertake research on methods to estimate temperatures of the surfaces most relevant to a specific problem based on the remote LST measurement, e.g., LST of roads and walls for health-related studies, LST of walls and roofs for building energy consumption studies; (2) utilize meteorological data obtained from published work or other accessible sources to identify the changing trend of rural temperatures which can represent temperature changes under climate change; (3) expand the sample size (the number of cities) of each climate

zone (4) apply geospatial regression models (e.g., geographically weighted regression); to quantify the relationship between multiple driving factors (e.g., building morphology, meteorological and socio-economic factors) and SUHI intensity and extent.

5. Conclusion

This study proposed an improved LCZ mapping method with a temporal consistency check and generated multi-temporal LCZ maps of large Chinese cities from 2000 to 2015. Based on the LCZ data, this research examined the spatial-temporal characteristics of intra-urban SUHI intensity and SUHI extent; SUHI extent was quantified by a proposed buffer-based approach. The main findings can be summarized as follows:

(1) The improved LCZ classification method classifies LCZ classes, particularly built types, more accurately in a complex urban context. The buffer-based approach quantifies the SUHI extent more accurately and can depict both single-core and multi-core urban development. (2) Obvious spatial-temporal patterns of intra-urban SUHI intensity and SUHI extent were observed—temporally, peak during summer days and low values in winter; spatially, decreasing with background climate becoming warm and wet. Additionally, SUHI extent increases with a rising urban area, particularly the area of LCZ 1, while its growth rate is slower than that of urban areas. (3) Regardless of background climate, LCZ 1 presents the highest SUHI intensity and significantly affects SUHI extent. LCZ 4 displays relatively low SUHI intensity when accommodating a similar population as LCZ 1, while it is still positively correlated to SUHI expansion. (4) In planning practice, restricting the area of LCZ 1 and properly arranging LCZ 4 will help mitigate urban heat from both perspectives of intensity and extent.

Based on quantitative analysis, this work provides evidence-based planning strategies for urban planners, architects and related decision-makers to mitigate SUHI. Mitigating urban heat helps improve health and socioeconomic conditions by reducing the thermal radiant loading on residents, thereby decreasing the morbidity of heat-related illnesses (e.g., heatstroke) and reducing energy consumption for cooling demand in summer. Our findings are beneficial for not only Chinese cities but also other cities undergoing or will experience rapid urbanization to mitigate urban heat and create comfort-oriented communities.

CRediT authorship contribution statement

Ran Wang: Writing – original draft, Methodology, Formal analysis, Conceptualization. **James Voogt:** Writing – review & editing, Investigation, Formal analysis. **Chao Ren:** Writing – review & editing, Supervision. **Edward Ng:** Writing – review & editing, Supervision.

Declaration of competing interest

The authors declare that they have no known competing financial interests or personal relationships that could have appeared to influence the work reported in this paper.

Data availability

Data will be made available on request.

Acknowledgments

This work is supported by the Postgraduate Studentship (PGS) 1155050998/Ph.D./ARD from The Chinese University of Hong Kong.

Appendix

Table A.1

Detailed information of target cities [57,58].

City	Geographical region	China architectural climate zone	Leading urban agglomeration	Administrative level	Function	Terrain	Urban population (10000 persons)		Built-up area (km ²)	
							2000	2015	2000	2015
Shenyang	Northeastern	SCR	Central-and-Southern Liaoning Jing-jin-ji	Provincial capital	Transportation and economic centers of northeastern China	The majority is smooth	506.6	667.8	217	465
Beijing	Northern	CR	Guangzhong	The national capital, municipality	Political, cultural and transportation center of China	Mountains and hills: around 62% of the total area	1057.06	1877.70	488	1401
Xi'an	Northwestern	CR	Yangtze River Delta	Provincial capital	Transportation, industrial, educational, and research center of northwestern China	Mountains at the south, plain at the north	450.36	635.68	187	501
Shanghai	Eastern	HSCW	Chengyu	Municipality	Economic, science and technology and cultural center of China	Smooth, average elevation: 4 m	1306.50	2115.78	550	998
Chongqing	Western	HSCW	The middle reaches of the Yangtze River	Municipality	Regional economic and transportation center of southwestern China	Mountains or hills: >80% of the total area	1014.18	1838.29	262	1329
Wuhan	Central	HSCW	Guangzhou-Hong Kong-Macau	Provincial capital	Economic, educational, innovative center of central China, inland transport hub	Rivers and lakes: nearly 25% of the total area	657.13	842.36	210	566
Guangzhou	Southeastern	HSWW	Guangzhou-Hong Kong-Macau	Provincial capital	Regional socioeconomic center of southeastern China	Hills and alluvial plain	835.18	1154.75	431	1237
Shenzhen	Southeastern	HSWW	Guangzhou-Hong Kong-Macau	Special economic zone	Financial, innovative, high-tech-industry-leading center of China	Hills and coastal plain	648.37	1137.87	136	900

Note: China architectural climate zone: SCR=Severe cold region, CR=Cold region, HSCW=Region with hot summer and cold winter, HSWW=Region with hot summer and warm winter.

Table A.2

Background climate (annual seasonal mean air temperature, precipitation and relative humidity) of eight large cities.

City	China architectural climate zone	Summer			Winter		
		AirT	P	RH	AirT	P	RH
Shenyang	SCR	23.99	372.25	75.26	-9.70	30.25	61.85
Beijing	CR	25.56	312.28	68.43	-4.53	11.75	48.33
Xi'an	CR	25.01	264.53	72.81	1.11	14.43	64.95
Shanghai	HSCW	27.40	538.80	75.64	5.97	195.65	70.92
Chongqing	HSCW	27.28	524.75	76.00	9.37	51.73	75.84
Wuhan	HSCW	28.00	486.10	75.82	5.35	148.35	74.79
Guangzhou	HSWW	28.52	882.33	76.83	14.69	120.58	70.23
Shenzhen	HSWW	28.75	941.48	76.32	16.35	122.18	70.03

Source: China Meteorological Administration.

Note: AirT—air temperature (°C), P—precipitation (mm), RH—relative humidity (%).

Table A.3

Spectral indices used as input data in LCZ mapping.

Indices	Equation	Notes	Reference
NDVI	$NDVI = (\rho_{NIR} - \rho_{red}) / (\rho_{NIR} + \rho_{red})$	Landsat 5: NIR—band 4, Red—band 3 Landsat 8: NIR—band 5, Red—band 4	[3]
NDBaI	$NDBaI = (\rho_{SWIR1} - \rho_{TIR}) / (\rho_{SWIR1} + \rho_{TIR})$	Landsat 5: SWIR 1—band 5, TIR—band 6 Landsat 8: SWIR 1—band 6, TIR—band 10	[4]
NDBI	$NDBI = (\rho_{MIR} - \rho_{NIR}) / (\rho_{MIR} + \rho_{NIR})$	Landsat 5: MIR—band 5, NIR—band 4 Landsat 8: MIR—band 6, NIR—band 5	[5]
NDWI	$NDWI = (\rho_{Green} - \rho_{NIR}) / (\rho_{Green} + \rho_{NIR})$	Landsat 5: Green—band 2, NIR—band 4 Landsat 8: Green—band 3, NIR—band 5	[6]

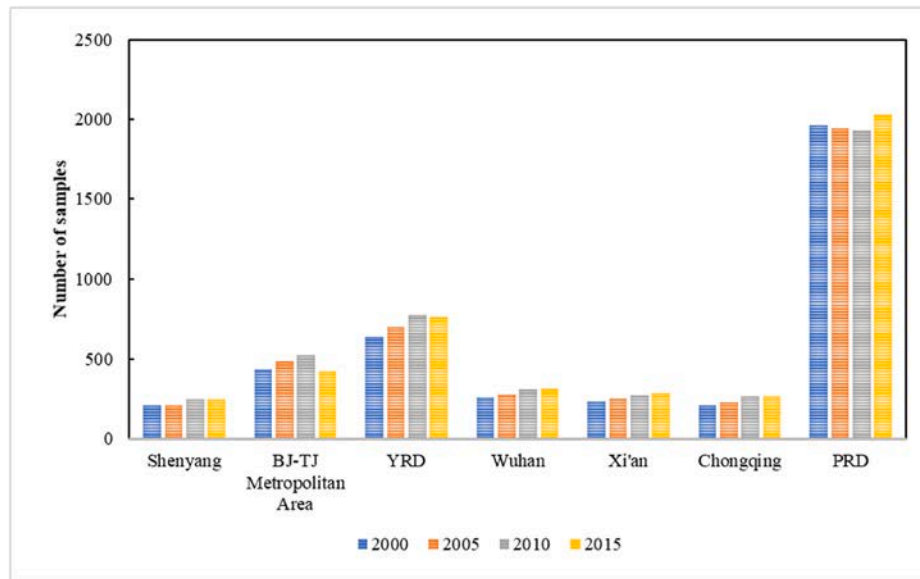


Fig. A1. The Number of training samples selected for study targets in 2000, 2005, 2010 and 2015. BJ-TJ: Beijing-Tianjin, YRD: Yangtze River Delta (Shanghai included), PRD: Pearl River Delta (Guangzhou and Shenzhen included)..

Table A.4
Sensitivity of SUHIE under different buffer distances based on SD

Buffer distance (m)	50–250	300–500	550–750	800–1000
SD	4.22	45.02	51.49	89.95

Table A.5

OA, OAn, OAu of each large Chinese city in 2000, 2005, 2010 and 2015 as well as the mean and standard deviation (SD). City name: SY—Shenyang, BJ—Beijing, XA—Xi'an, WH—Wuhan, CQ—Chongqing, YRD—Yangtze River Delta (Shanghai included), PRD—Pearl River Delta (Guangzhou and Shenzhen included)

Year	Accuracy assessment index	SY	BJ	YRD	WH	XA	CQ	PRD	Mean	SD
2000	OA	89.52	83.98	81.94	89.59	87.52	93.91	87.13	87.74	3.64
	OAn	92.72	93.86	91.12	93.50	88.27	95.46	89.98	92.49	2.29
	OAu	76.61	67.52	65.59	75.56	78.57	83.33	80.91	74.53	6.13
2005	OA	90.42	88.45	82.93	92.64	87.79	93.27	85.75	89.25	3.43
	OAn	93.29	96.28	91.66	95.19	89.22	95.82	88.25	93.58	2.98
	OAu	78.94	72.93	67.73	84.66	75.44	80.54	81.25	76.71	5.31
2010	OA	88.87	86.85	80.92	89.61	86.68	89.71	87.76	87.11	2.81
	OAn	93.21	95.22	91.78	94.18	88.96	95.42	90.13	93.13	2.32
	OAu	76.48	71.43	67.75	79.16	72.12	75.85	83.21	73.80	4.79
2015	OA	86.29	93.46	82.71	89.30	87.81	91.29	91.87	88.48	3.42
	OAn	90.73	94.81	92.54	93.40	89.85	96.40	94.85	92.96	2.18
	OAu	75.74	82.02	69.46	79.50	76.30	77.80	86.85	76.80	5.03

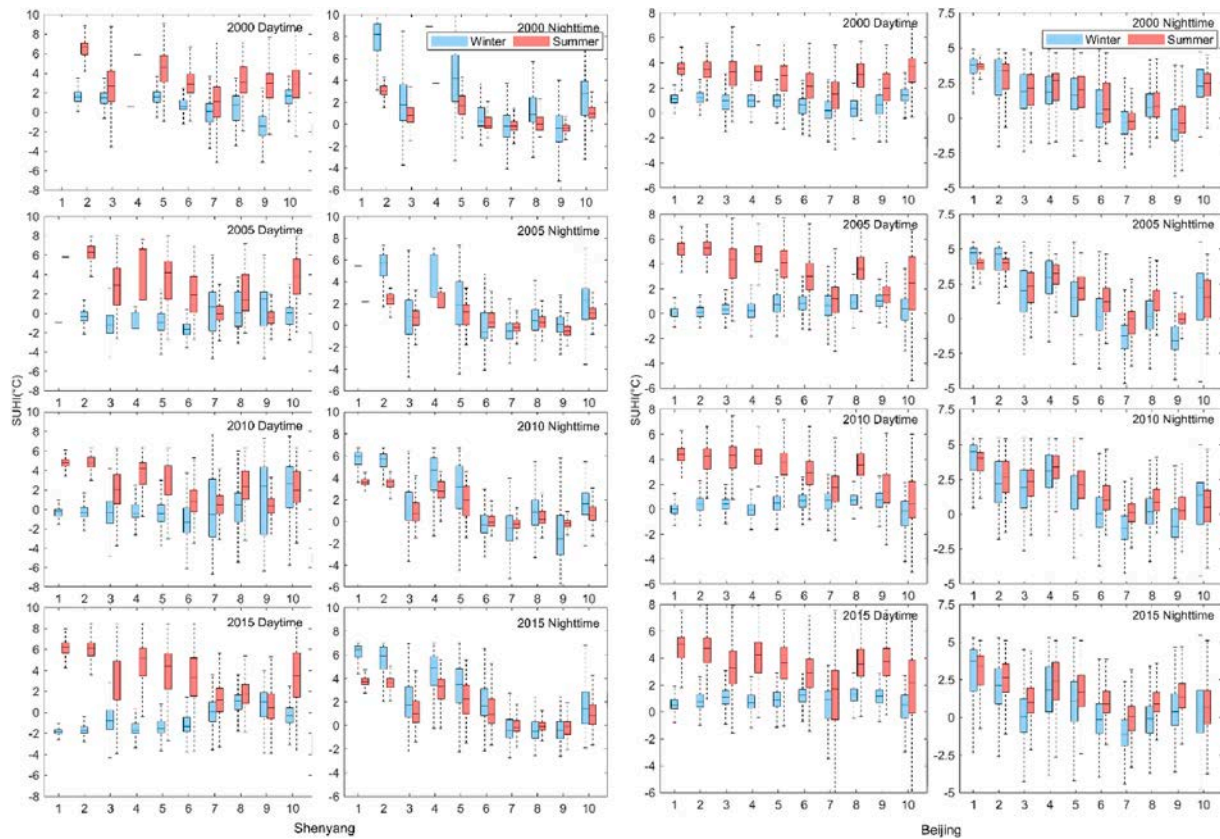


Fig. A2. Box plots of SUHI intensity for 10 LCZ built types in eight large Chinese cities in winter and summer seasons during daytime and nighttime. The black line inside the box represents median LST, while the bottom and top of the box are the first and third quartile respectively. The upper and lower whiskers signify the maximum LST and minimum LST within 1.5 IQR (interquartile range: the first to the third quartile). The x-axis refers to LCZ classes. The SUHI (°C) is calculated based on $T_{LCZ \text{ built type}} - T_{LCZ \text{ D}}$.

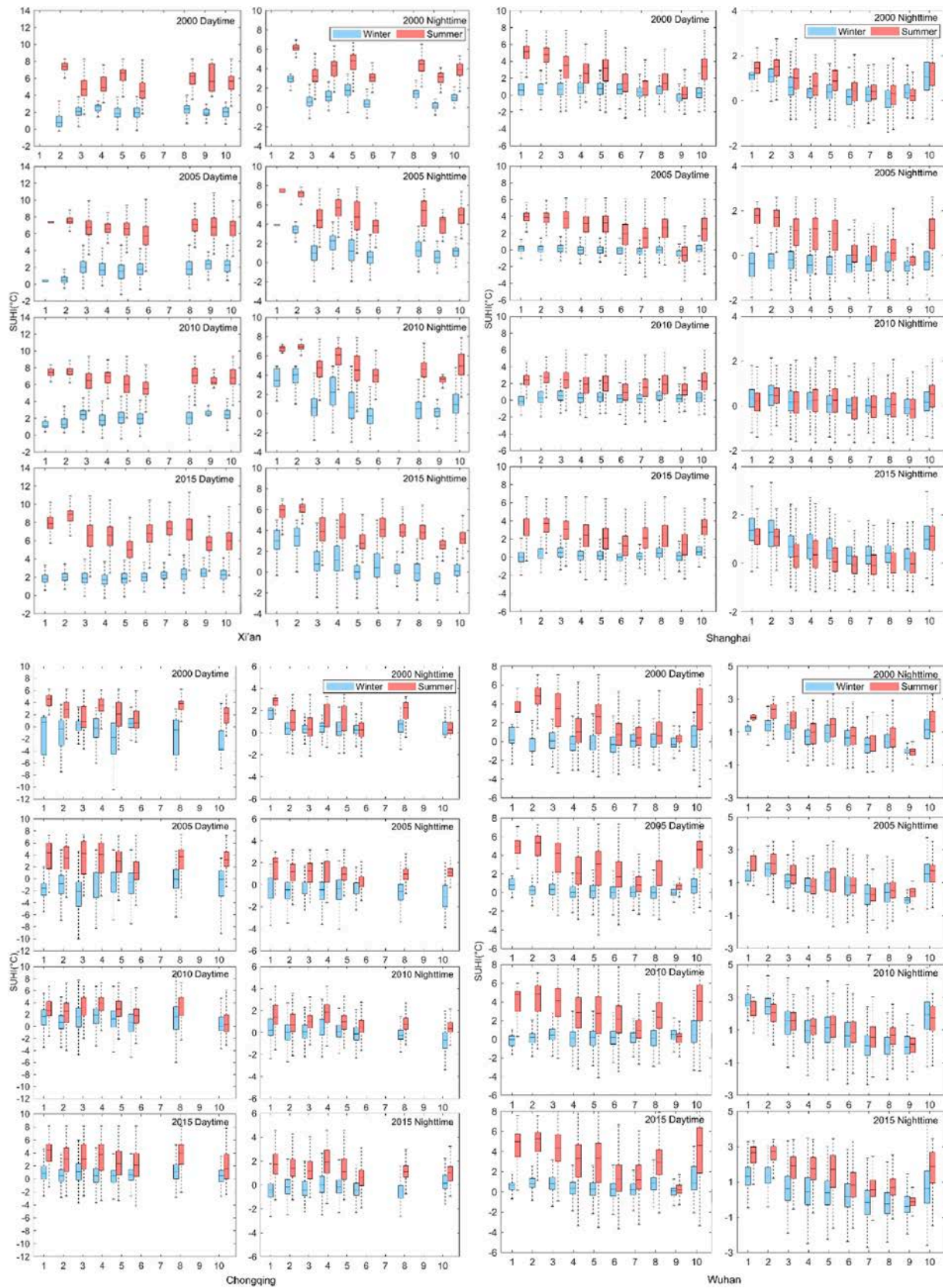


Fig. A2. (continued).

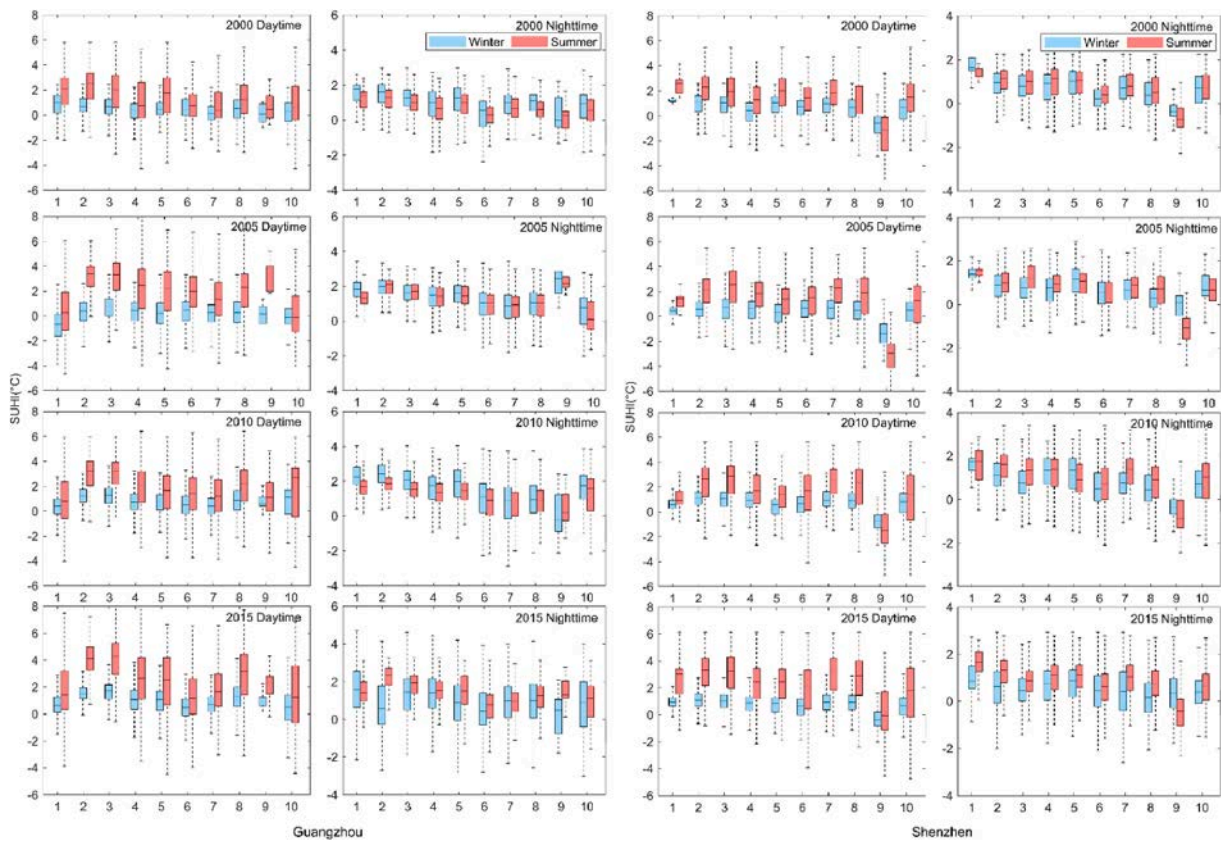


Fig. A2. (continued).

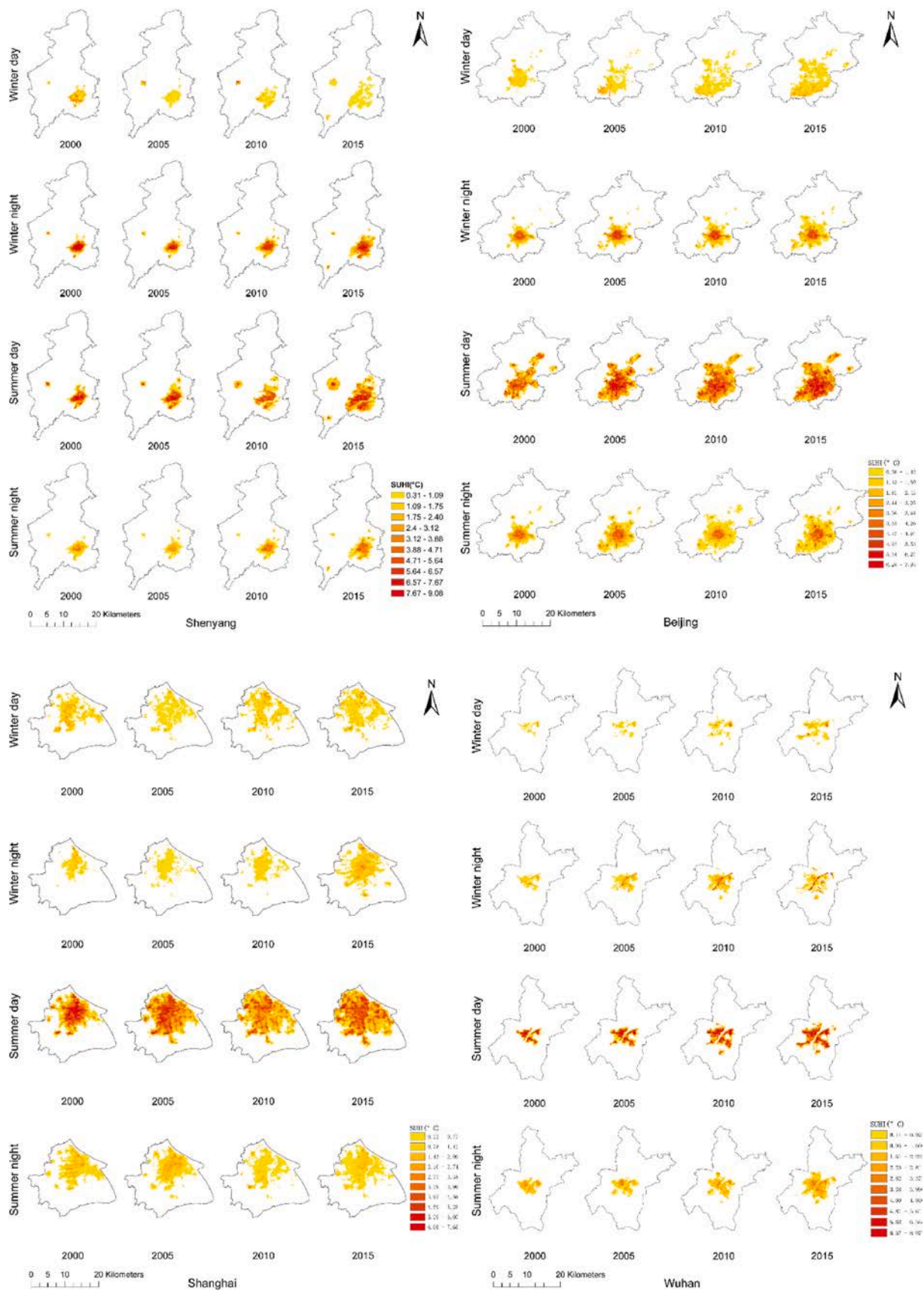


Fig. A3. Daytime and nighttime spatial distribution of significant SUHI effect (i.e., SUHI extent) in large Chinese cities during winter and summer from 2000 to 2015 .

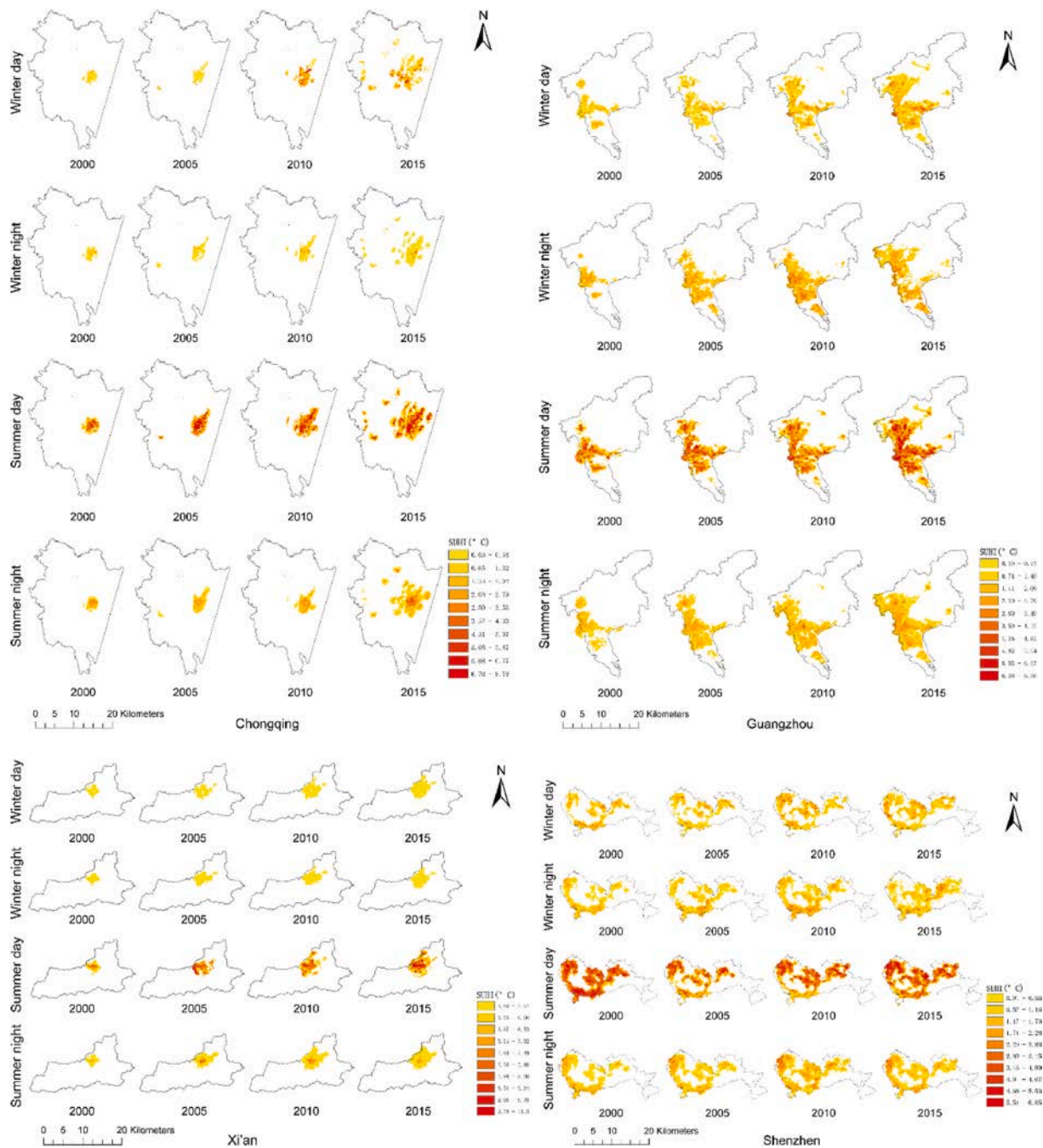


Fig. A3. (continued).

References

[1] J. Geletić, M. Lehnert, S. Savić, D. Milošević, Inter-/intra-zonal seasonal variability of the surface urban heat island based on local climate zones in three central European cities, *Build. Environ.* 156 (2019) 21–32, <https://doi.org/10.1016/j.buildenv.2019.04.011>.

[2] Q. Yang, X. Huang, Q. Tang, The footprint of urban heat island effect in 302 Chinese cities: temporal trends and associated factors, *Sci. Total Environ.* 655 (2019) 652–662, <https://doi.org/10.1016/j.scitotenv.2018.11.171>.

[3] B. Mashhoodi, D. Stead, A. van Timmeren, Land surface temperature and households' energy consumption: who is affected and where? *Appl. Geogr.* 114 (2020), 102125 <https://doi.org/10.1016/j.apgeog.2019.102125>.

[4] K. Laaidi, A. Zeghnoun, B. Dousset, P. Bretin, S. Vandentorren, E. Giraudet, P. Beaudeau, The impact of heat islands on mortality in Paris during the August 2003 heat wave, *Environ. Health Perspect.* 120 (2) (2012) 254–259, <https://doi.org/10.1289/ehp.1103532>.

[5] National Bureau of Statistics of China, The Director of the National Bureau of Statistics Answers Reporters' Questions on the Operation of the National Economy in 2020, 2021. http://www.stats.gov.cn/tjsj/sjjd/202101/t20210118_1812480.html.

[6] United Nations, *World Urbanization Prospects: the 2018 Revision*, United Nations Department of Economics and Social Affairs, Population Division, New York, NY, USA, 2018.

[7] I.D. Stewart, T.R. Oke, Local climate zones for urban temperature studies, *Bull. Am. Meteorol. Soc.* 93 (12) (2012) 1879–1900, <https://doi.org/10.1175/BAMS-D-11-00019.1>.

[8] B. Bechtel, P.J. Alexander, J. Böhner, J. Ching, O. Conrad, J. Feddema, G. Mills, L. See, I. Stewart, Mapping local climate zones for a worldwide database of the form and function of cities, *ISPRS Int. J. Geo-Inf.* 4 (1) (2015) 199–219, <https://doi.org/10.3390/ijgi4010199>.

[9] M. Cai, C. Ren, Y. Xu, K.K.-L. Lau, R. Wang, Investigating the relationship between local climate zone and land surface temperature using an improved WUDAPT methodology-A case study of Yangtze River Delta, China, *Urban Clim.* 24 (2018) 485–502, <https://doi.org/10.1016/j.uclim.2017.05.010>.

- [10] J. Rosentreter, R. Hagenseker, B. Waske, Towards large-scale mapping of local climate zones using multitemporal Sentinel 2 data and convolutional neural networks, *Remote Sens. Environ.* 237 (2020), 111472, <https://doi.org/10.1016/j.rse.2019.111472>.
- [11] C. Dian, R. Pongrácz, Z. Dezsó, J. Bartholy, Annual and monthly analysis of surface urban heat island intensity with respect to the local climate zones in Budapest, *Urban Clim.* 31 (2020), 100573, <https://doi.org/10.1016/j.uclim.2019.100573>.
- [12] C. Ren, M. Cai, X. Li, L. Zhang, R. Wang, Y. Xu, E. Ng, Assessment of local climate zone classification maps of cities in China and feasible refinements, *Sci. Rep.* 9 (1) (2019), 18848, <https://doi.org/10.1038/s41598-019-55444-9>.
- [13] C. Wang, A. Middel, S.W. Myint, S. Kaplan, A.J. Brazel, J. Lukaszczuk, Assessing local climate zones in arid cities: the case of Phoenix, Arizona and Las Vegas, Nevada, *ISPRS J. Photogrammetry Remote Sens.* 141 (2018) 59–71, <https://doi.org/10.1016/j.isprsjprs.2018.04.009>.
- [14] L.C. Hay Chung, J. Xie, C. Ren, Improved machine-learning mapping of local climate zones in metropolitan areas using composite Earth observation data in Google Earth Engine, *Build. Environ.* 199 (2021), 107879, <https://doi.org/10.1016/j.buildenv.2021.107879>.
- [15] M. Demuzere, S. Hankey, G. Mills, W. Zhang, T. Lu, B. Bechtel, Combining expert and crowd-sourced training data to map urban form and functions for the continental US, *Sci. Data* 7 (1) (2020) 1–13, <https://doi.org/10.1038/s41597-020-00605-z>.
- [16] M. Demuzere, B. Bechtel, A. Middel, G. Mills, Mapping Europe into local climate zones, *PLoS One* 14 (4) (2019), e0214474, <https://doi.org/10.1371/journal.pone.0214474>.
- [17] R. Wang, M. Cai, C. Ren, B. Bechtel, Y. Xu, E. Ng, Detecting multi-temporal land cover change and land surface temperature in Pearl River Delta by adopting local climate zone, *Urban Clim.* 28 (2019), 100455, <https://doi.org/10.1016/j.uclim.2019.100455>.
- [18] J. Peng, Y. Hu, J. Dong, Q. Liu, Y. Liu, Quantifying spatial morphology and connectivity of urban heat islands in a megacity: a radius approach, *Sci. Total Environ.* 714 (2020), 136792, <https://doi.org/10.1016/j.scitotenv.2020.136792>.
- [19] J. Quan, Y. Chen, W. Zhan, J. Wang, J. Voogt, M. Wang, Multi-temporal trajectory of the urban heat island centroid in Beijing, China based on a Gaussian volume model, *Remote Sens. Environ.* 149 (2014) 33–46, <https://doi.org/10.1016/j.rse.2014.03.037>.
- [20] J. Zhou, Y. Chen, J. Wang, W. Zhan, Maximum nighttime urban heat island (UHI) intensity simulation by integrating remotely sensed data and meteorological observations, *IEEE J. Sel. Top. Appl. Earth Obs. Rem. Sens.* 4 (1) (2010) 138–146, <https://doi.org/10.1109/JSTARS.2010.2070871>.
- [21] D.R. Streutker, A remote sensing study of the urban heat island of Houston, Texas, *Int. J. Rem. Sens.* 23 (13) (2002) 2595–2608, <https://doi.org/10.1080/10431160110115023>.
- [22] Ministry of Housing and Urban-Rural Development, *Uniform Standard for Civil Building Design*, 2019. Beijing.
- [23] Ministry of Housing and Urban-Rural Development, *Standard of Climatic Regionalization for Architecture*, 1993. Beijing.
- [24] T. Purevdorj, R. Tateishi, T. Ishiyama, Y. Honda, Relationships between percent vegetation cover and vegetation indices, *Int. J. Rem. Sens.* 19 (18) (1998) 3519–3535, <https://doi.org/10.1080/014311698213795>.
- [25] H. Zhao, X. Chen, Use of normalized difference bareness index in quickly mapping bare areas from TM/ETM+, *IEEE Int. Geosci. Remote Sens. Symp.* (2005) 1666, <https://doi.org/10.1109/IGARSS.2005.1526319>.
- [26] Y. Zha, J. Gao, S. Ni, Use of normalized difference built-up index in automatically mapping urban areas from TM imagery, *Int. J. Rem. Sens.* 24 (3) (2003) 583–594, <https://doi.org/10.1080/01431160304987>.
- [27] S.K. McFeeters, The use of the Normalized Difference Water Index (NDWI) in the delineation of open water features, *Int. J. Rem. Sens.* 17 (7) (1996) 1425–1432, <https://doi.org/10.1080/01431169608948714>.
- [28] T. Tadono, H. Nagai, H. Ishida, F. Oda, S. Naito, K. Minakawa, H. Iwamoto, *Generation of the 30 M-mesh global digital surface model by alos prism*, international archives of the photogrammetry, *Remote Sense. Spatial Info. Sci.* 41 (2016).
- [29] T.G. Farr, P.A. Rosen, E. Caro, R. Crippen, R. Duren, S. Hensley, M. Kobrick, M. Paller, E. Rodriguez, L. Roth, D. Seal, S. Shaffer, J. Shimada, J. Umland, M. Werner, M. Oskin, D. Burbank, D. Alsdorf, The Shuttle radar topography mission, *Rev. Geophys.* 45 (2) (2007), <https://doi.org/10.1029/2005RG000183>.
- [30] J.J. Danielson, D.B. Gesch, *Global Multi-Resolution Terrain Elevation Data 2010 (GMTED2010)*, US Department of the Interior, US Geological Survey, 2011.
- [31] L. Breiman, Random forests, *Mach. Learn.* 45 (1) (2001) 5–32, <https://doi.org/10.1023/A:10109333404324>.
- [32] A. Schneider, C. Mertes, Expansion and growth in Chinese cities, 1978–2010, *Environ. Res. Lett.* 9 (2) (2014), 024008, <https://doi.org/10.1088/1748-9326/9/2/024008>.
- [33] Z. Wan, New refinements and validation of the MODIS land-surface temperature/emissivity products, *Remote Sens. Environ.* 112 (1) (2008) 59–74, <https://doi.org/10.1016/j.rse.2006.06.026>.
- [34] M.L. Imhoff, P. Zhang, R.E. Wolfe, L. Bounoua, Remote sensing of the urban heat island effect across biomes in the continental USA, *Remote Sens. Environ.* 114 (3) (2010) 504–513, <https://doi.org/10.1016/j.rse.2009.10.008>.
- [35] G.B. Anderson, M.L. Bell, Heat waves in the United States: mortality risk during heat waves and effect modification by heat wave characteristics in 43 US communities, *Environ. Health Perspect.* 119 (2) (2011) 210–218, <https://doi.org/10.1289/ehp.1002313>.
- [36] D. García-León, A. Casanueva, G. Standardi, A. Burgstall, A.D. Flouris, L. Nybo, Current and projected regional economic impacts of heatwaves in Europe, *Nat. Commun.* 12 (1) (2021) 1–10, <https://doi.org/10.1038/s41467-021-26050-z>.
- [37] F. Rong, *Impact of Urban Sprawl on US Residential Energy Use*, 2006.
- [38] B. Bechtel, M. Demuzere, G. Mills, W. Zhan, P. Sismanidis, C. Small, J. Voogt, SUHI analysis using Local Climate Zones-A comparison of 50 cities, *Urban Clim.* 28 (2019), 100451, <https://doi.org/10.1016/j.uclim.2019.01.005>.
- [39] W. Wu, S. Zhao, C. Zhu, J. Jiang, A comparative study of urban expansion in Beijing, Tianjin and Shijiazhuang over the past three decades, *Landsc. Urban Plann.* 134 (2015) 93–106, <https://doi.org/10.1016/j.landurbplan.2014.10.010>.
- [40] S. Peng, S. Piao, P. Ciais, P. Friedlingstein, C. Ottle, F.o.-M. Bréon, H. Nan, L. Zhou, R.B. Myneni, Surface urban heat island across 419 global big cities, *Environ. Sci. Technol.* 46 (2) (2012) 696–703, <https://doi.org/10.1021/es2030438>.
- [41] S. Liu, Q. Shi, Local climate zone mapping as remote sensing scene classification using deep learning: a case study of metropolitan China, *ISPRS J. Photogrammetry Remote Sens.* 164 (2020) 229–242, <https://doi.org/10.1016/j.isprsjprs.2020.04.008>.
- [42] Z. Qiao, C. Wu, D. Zhao, X. Xu, J. Yang, L. Feng, Z. Sun, L. Liu, Determining the boundary and probability of surface urban heat island footprint based on a logistic model, *Rem. Sens.* 11 (11) (2019) 1368, <https://www.mdpi.com/2072-4292/11/11/1368>.
- [43] H. Du, D. Wang, Y. Wang, X. Zhao, F. Qin, H. Jiang, Y. Cai, Influences of land cover types, meteorological conditions, anthropogenic heat and urban area on surface urban heat island in the Yangtze River Delta Urban Agglomeration, *Sci. Total Environ.* 571 (2016) 461–470, <https://doi.org/10.1016/j.scitotenv.2016.07.012>.
- [44] Y. Hu, M. Hou, G. Jia, C. Zhao, X. Zhen, Y. Xu, Comparison of surface and canopy urban heat islands within megacities of eastern China, *ISPRS J. Photogrammetry Remote Sens.* 156 (2019) 160–168, <https://doi.org/10.1016/j.isprsjprs.2019.08.012>.
- [45] D. Zhou, S. Zhao, S. Liu, L. Zhang, C. Zhu, Surface urban heat island in China's 32 major cities: spatial patterns and drivers, *Remote Sens. Environ.* 152 (2014) 51–61, <https://doi.org/10.1016/j.rse.2014.05.017>.
- [46] D. Zhou, S. Zhao, L. Zhang, G. Sun, Y. Liu, The footprint of urban heat island effect in China, *Sci. Rep.* 5 (1) (2015) 1–11, <https://doi.org/10.1038/srep11160>.
- [47] J. Lai, W. Zhan, J. Voogt, J. Quan, F. Huang, J. Zhou, B. Bechtel, L. Hu, K. Wang, C. Cao, Meteorological controls on daily variations of nighttime surface urban heat islands, *Remote Sens. Environ.* 253 (2021), 112198, <https://doi.org/10.1016/j.rse.2020.112198>.
- [48] M. Jin, R.E. Dickinson, D. Zhang, The footprint of urban areas on global climate as characterized by MODIS, *J. Clim.* 18 (10) (2005) 1551–1565, <https://doi.org/10.1175/JCLI3334.1>.
- [49] A.J. Arnfield, Two decades of urban climate research: a review of turbulence, exchanges of energy and water, and the urban heat island, *Int. J. Climatol.* 23 (1) (2003) 1–26, <https://doi.org/10.1002/joc.859>.
- [50] Y. Li, Y. Sun, J. Li, C. Gao, Socioeconomic drivers of urban heat island effect: empirical evidence from major Chinese cities, *Sustain. Cities Soc.* 63 (2020), 102425, <https://doi.org/10.1016/j.scs.2020.102425>.
- [51] T.R. Oke, G. Mills, A. Christen, J.A. Voogt, *Urban Climates*, Cambridge University Press, 2017.
- [52] I.D. Stewart, E.S. Kravynhoff, J.A. Voogt, J.A. Lachapelle, M.A. Allen, A. M. Broadbent, Time evolution of the surface urban heat island, *Earth's Future* 9 (10) (2021), e2021EF002178, <https://doi.org/10.1029/2021EF002178>.
- [53] X. Chen, J. Yang, C. Ren, S. Jeong, Y. Shi, Standardizing thermal contrast among local climate zones at a continental scale: implications for cool neighborhoods, *Build. Environ.* 197 (2021), 107878, <https://doi.org/10.1016/j.buildenv.2021.107878>.
- [54] F. Leconte, J. Bouyer, R. Claverie, M. Pétrissans, Using Local Climate Zone scheme for UHI assessment: evaluation of the method using mobile measurements, *Build. Environ.* 83 (2015) 39–49, <https://doi.org/10.1016/j.buildenv.2014.05.005>.
- [55] Development Research Center of the State Council of China, World Bank Group, China: Promote Effective, Diverse, and Sustainable Urbanization, Beijing, 2014.
- [56] A. Martilli, E.S. Kravynhoff, N. Nazarian, Is the Urban Heat Island intensity relevant for heat mitigation studies? *Urban Clim.* 31 (2020), 100541, <https://doi.org/10.1016/j.uclim.2019.100541>.
- [57] National Bureau of Statistics of China, *China City Statistical Yearbook*, China Statistics Press, Beijing, 2001.
- [58] National Bureau of Statistics of China, *China City Statistical Yearbook*, China Statistics Press, Beijing, 2016.